

Article

Entropy Generation in MHD Mixed Convection Non-Newtonian Second-Grade Nanoliquid Thin Film Flow through a Porous Medium with Chemical Reaction and Stratification

Noor Saeed Khan ¹, Zahir Shah ¹, Saeed Islam ¹, Ilyas Khan ^{2,*} and Tawfeeq Abdullah Alkanhal ³ and Iskander Tlili ⁴

¹ Department of Mathematics, Abdul Wali Khan University, Mardan 23200, Khyber Pakhtunkhwa, Pakistan; noorsaeedkhanhattak@gmail.com (N.S.K.); zahir1987@yahoo.com (Z.S.); saeedislam@awkum.edu.pk (S.I.)

² Faculty of Mathematics and Statistics, Ton Duc Thang University, Ho Chi Minh City 736464, Vietnam

³ Department of Mechatronics and System Engineering, College of Engineering, Majmaah University, Al-Majmaah 11952, Saudi Arabia; t.alkanhal@mu.edu.sa

⁴ Department of Mechanical and Industrial Engineering, College of Engineering, Majmaah University, Al-Majmaah 11952, Saudi Arabia; i.tlili@mu.edu.sa

* Correspondence: ilyaskhan@tdt.edu.vn

Received: 8 December 2018; Accepted: 30 January 2019; Published: 1 February 2019



Abstract: Chemical reaction in mixed convection magnetohydrodynamic second grade nanoliquid thin film flow through a porous medium containing nanoparticles and gyrotactic microorganisms is considered with entropy generation. The stratification phenomena, heat and mass transfer simultaneously take place within system. Microorganisms are utilized to stabilize the suspended nanoparticles through bioconvection. For the chemical reaction of species, the mass transfer increases. The governing equations of the problem are transformed to nonlinear differential equations through similarity variables, which are solved through a well known scheme called homotopy analysis method. The solution is expressed through graphs and illustrations which show the influences of all the parameters. The residual error graphs elucidate the authentication of the present work.

Keywords: entropy generation; chemical reaction; thin film; magnetohydrodynamic; gravity-driven; second-grade nanofluid; mixed convection; passively controlled nanofluid model; gyrotactic microorganisms; convective boundary conditions; residual errors; homotopy analysis method

1. Introduction

Entropy is a thermodynamic quantity representing the unavailability of a system's thermal energy for conversion into mechanical work, often interpreted as the degree of disorder or randomness in the system. Entropy generation is an important part of the mechanical system. In the context of the present situation, irreversibility (entropy generation) is reliant to heat transmission, viscous dissipation and effects of magnetic field as well as diffusion. Irreversibility is studied with a sharp rate. The present study also discusses bioconvection and chemical reaction. Bio-convection is associated with a macroscopic flow of convecting fluid under the effect of density gradients due to hydrodynamic propulsion such as swimming of motile microorganisms. Mixed convection has several applications including heat dismissal into the atmosphere like lakes, rivers and seas. It is also utilized in the storage of thermal energy like

solar ponds and heat transfer thermal sources such as the condensers of power plants. The applications of biosynthesized nanoparticles in a wide spectrum of potential areas are targeted drug delivery, cancer treatment gene therapy and DNA analysis, antibacterial agents, biosensors, enhancing reaction rates, separation science and magnetic resonance imaging (MRI). Entropy generation and bioconvection is a hot subject for scientists and researchers. Some published works and their few findings are given in Table 1.

Table 1. Some recent developments related to the topic under investigation.

Author Names	Author Works	Some Outcomes
Khan et al. [1]	Entropy generation	Entropy generation increases with Reynolds number
Ishaq et al. [2]	Entropy generation	Entropy generation decreases with Eyring-Powell parameter
Hayat et al. [3]	Entropy generation	Entropy generation increases with Reynolds number
Khan et al. [4]	Bioconvection	Bioconvection decreases with reduced heat transfer parameter
Zuhra et al. [5]	Bioconvection	Gyrotactic microorganisms depreciates with magnetic field parameter
Khan [6]	Bioconvection	Stratification increases with second-grade fluid parameter
Palwasha et al. [7]	Bioconvection	Stratification increases with gravitational forces
Raees et al. [8]	Bioconvection	Bioconvection depends on upper plate
Zuhra et al. [9]	Bioconvection	Microorganisms decrease with increasing Brownian motion parameter
Pedley [10]	Instability	Instability of the system is due to microorganisms
Xu et al. [11]	Mixed convection	Nanoparticles favor the mixed convection
Aziz et al. [12]	Free convection	Instability of the system increases due to microorganisms
Bhatti et al. [13]	Chemical reaction	Mass transfer increases with chemical reaction
Raees et al. [14]	Bioconvection'	Passively controlled nanofluid model provides better results
Ramzan et al. [15]	Chemical reaction	Mass transfer increases with chemical reaction
Anjalidevi [16]	Chemical reaction	Mass transfer increases with chemical reaction

The study of applied magnetic field plays a significant role in heat and mass transfer, controlling momentum in boundary layer nanofluid flow through a shrinking/stretching surface. Moreover, magnetohydrodynamics is utilized in diverse engineering applications like cooling of nuclear reactor, electromagnetic casting and plasma confinement. In microfluidics complexities, magnetohydrodynamics is helpful to create non-pulsating and continuous movement in the structure of complex micro-channels. In biomedical engineering, magnetohydrodynamics is applicable for magnetic drug targeting in cancer diseases. On behalf of these applications, Khan et al. [17] explored that due to the strong applied magnetic field, flow becomes slow and temperature becomes high. They also found the residual errors for the authentication of the solution. Palwasha et al. [18] discussed the intensified magnetic field which causes the Hall current effect in two dimensions case. They found that magnetic field effect is a highly dominant factor to the flow. Khan et al. [19] presented the study to show the effects of applied magnetic field on graphene nanoparticles in a thin film Eyring Powell nanofluid involving velocity slip condition. Their results reveal that the thermal conductivity increases with increasing the concentration of graphene nanoparticles. Zuhra et al. [20] also provided the study on graphene nanoparticles in two dimensional unsteady flow and heat transfer in thin liquid film non-Newtonian (Casson and Williamson) nanofluids suspension past a stretching sheet in the presence of transverse magnetic field and non-uniform heat source/sink. Their study shows that the temperature increases with temperature dependent heat source sink parameter. Khan et al. [21] analyzed the magnetohydrodynamic study in cylindrical coordinates for nanoliquid thin film using spraying phenomenon in thermal system. Apart from various effects of different parameters on different profiles, they also discussed the pressure role in the system. Focusing on the MHD flow, Khan et al. [22] presented Brownian motion and thermophoresis effects on MHD mixed convective thin film second-grade nanofluid flow with Hall effect and heat transfer past a stretching sheet, manifesting that the flow becomes three dimensional due to Hall effect.

The study of motion through a porous space is also very important in engineering and industrial processes. A porous media is a material having pores, i.e., oxides and metals, where these pores are covered with a fluid. Such type of motion has two main benefits, as its area of dissipation is higher as compared to conventional fins that improve the heat convection. Further, the regular flow of a fluid along the whole individual beads blends the fluid effectively. The nanofluid flow through a porous media reveals enhanced thermal properties, i.e., convective heat transfer coefficients as compared with a base material and higher thermal conductivity. Consequently, a porous media having nanoparticles plays a vital role in the enhancement of heat transfer and this mechanism is very important from an application and theoretical point of view. Such types of flow can be seen in filtration, oil flow, heat exchangers, drying process and geothermal systems. Moreover, nanofluid flow through a porous media has many applications in thermal engineering which are favorable to improve the thermal properties of lubricants and oil, electronic cooling equipment and vehicle cooling. Applying Navier-Stokes equations to the physical problems, Khan et al. [23] examined the important role of flow and transfer in a second-grade fluid through a porous medium past a stretching sheet in which the porous medium carries a leading role. Their results show a close agreement with the published work. It is very important to explain how nanofluid flow is possible in a porous medium. Thus, without special precautions, nanoparticles will be simply absorbed by the porous matrix. Basically, the porous matrix will work as a filter for nanoparticles. This situation has been described, explained and modeled in the paper by Wu et al. [24]. The physical situation described in this paper reveals that the work on porous media filled by nanofluids is not just a mathematical challenge, but is based on a deep physical understanding of nanofluid flows. This demonstrates that we are simulating here a real physics problem of mixed convection flow and heat transfer in a porous medium filled by a nanofluid. Kuznetsova [25] has compiled the studies on the developments of bioconvection in porous media caused by either gyrotactic or oxytactic microorganisms, with the limitation of average pore size is larger than the size of a microorganism, which allows the smooth movement of the microorganisms. Tham et al. [26] numerically studied the steady mixed convection boundary layer flow on a horizontal circular cylinder with a constant surface temperature embedded in a porous medium saturated by a nanofluid containing both nanoparticles and gyrotactic microorganisms in a stream flowing vertically upwards for both cases of a heated and cooled cylinder. The objective of that paper is to understand the behavior of nanofluid suspensions containing nanoparticles, gyrotactic microorganisms and entropy generation at the fundamental level.

Motivated from the above discussion, the present study discusses the entropy generation and mixed convection in gravity-driven MHD second grade nanofluid flow containing both nanoparticles and gyrotactic microorganisms through a porous medium with chemical reaction along a convectively heated vertical surface. Employing suitable transformations, the basic governing equations of the problem are converted to dimensionless form which have been solved using a powerful analytic tool called Homotopy Analysis Method (HAM) [27]. The influences of all the pertinent parameters on velocity, temperature, nanoparticle concentration, density motile microorganisms and entropy generation profiles have been shown graphically and illustrated.

2. Methods

Basic Equations

A motion of a magnetohydrodynamic two dimensional, time independent, laminar and an incompressible second grade nanofluid falling downwards through a porous medium along a vertical solid surface due to gravity is considered. The uniform incoming flow on the right side of the plate has a constant temperature T_∞ at $x = 0$ and the nanofluid on the left side of the plate has another constant temperature T_f . To avoid the bioconvection instability, it is assumed that the nanofluid is dilute. In addition, the assumption is

taken for the stability of the nanoparticles suspended in the base fluid so that the nanoparticles do not agglomerate in the fluid. The passive control of nanoparticles volume fraction at the boundary (on the solid wall) is taken. It is assumed that the microorganisms have constant distributions on the wall. It is most important to note that the base fluid is water so that the microorganisms can survive. The assumption is also maintained that the existence of nanoparticles has few effects on the motion of the microorganisms. A transverse magnetic field of strength B_0 is applied in the positive y -direction, normal to the plate surface. There is no applied voltage and the magnetic Reynolds number is small, so the induced magnetic field and Hall effects are negligible. The physical model and coordinate system are shown in Figure 1.

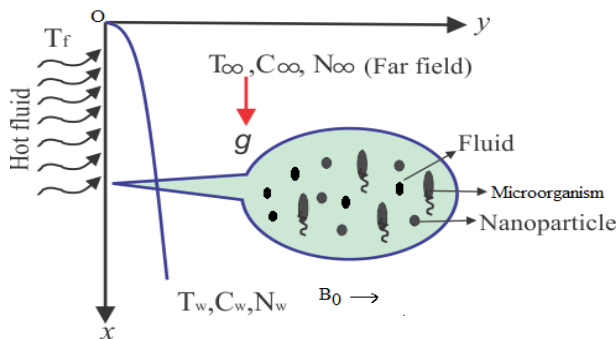


Figure 1. Geometry of the physical model and coordinates system.

Applying the above-mentioned assumptions, the equations for the nano-bioconvection model are written in the following form as in [4,13–15]

$$\frac{\partial u}{\partial x} + \frac{\partial v}{\partial y} = 0, \tag{1}$$

$$\rho_f \left(u \frac{\partial u}{\partial x} + v \frac{\partial u}{\partial y} \right) = \rho_f U \frac{dU}{dx} + \mu_f \frac{\partial^2 u}{\partial y^2} + \alpha_1 \left[\frac{\partial}{\partial x} \left(u \frac{\partial^2 u}{\partial y^2} \right) - \frac{\partial u}{\partial y} \frac{\partial^2 u}{\partial x \partial y} + v \frac{\partial^3 u}{\partial y^3} \right] + \left[(1 - C) \rho_{f\infty} g \beta (T - T_\infty) \right] - \left[(\rho_p - \rho_{f\infty}) g (C - C_\infty) \right] + \left[g (N - N_\infty) \gamma_{av} \Delta \rho \right] - \sigma B_0^2 u - \frac{\nu_f}{k} (u - U_\infty) - \frac{k^F}{\sqrt{k}} (u^2 - U_\infty^2), \tag{2}$$

$$u \frac{\partial T}{\partial x} + v \frac{\partial T}{\partial y} = \lambda \frac{\partial^2 T}{\partial y^2} + \tau \left[D_B \left(\frac{\partial C}{\partial y} \frac{\partial T}{\partial y} \right) + \left(\frac{D_T}{T_\infty} \right) \left(\frac{\partial T}{\partial y} \right)^2 \right], \tag{3}$$

$$u \frac{\partial C}{\partial x} + v \frac{\partial C}{\partial y} = \frac{D_B \partial^2 C}{\partial y^2} + \frac{D_T}{T_\infty} \frac{\partial^2 T}{\partial y^2} - k_r (C - C_\infty), \tag{4}$$

$$u \frac{\partial N}{\partial x} + v \frac{\partial N}{\partial y} + \frac{\partial (N \bar{v})}{\partial y} = D_n \frac{\partial^2 N}{\partial y^2}. \tag{5}$$

Here

$$\frac{dp}{dx} = \rho_f U \frac{dU}{dx}, \quad U = (2ax)^{\frac{1}{2}}, \tag{6}$$

where U is the free stream velocity, a is constant, u and v are the velocity components in the x - and y -directions. α_1 is the normal stress moduli, $\bar{v} = \left(\frac{bW_c}{\Delta C} \right) \frac{\partial C}{\partial y}$ is the average swimming velocity vector of the oxytactic microorganisms in which b is the chemotaxis constant and W_c is the maximum cell swimming

speed. The subscripts p, f and f_∞ denote respectively the solid particles, the nanofluid and the base fluid at far field. $\Delta\rho = \rho_{cell} - \rho_{f_\infty}$ is the density difference between a cell and base fluid density at far field, μ_f is the dynamic viscosity, γ_{av} is the average volume of microorganisms, σ is the electrical conductivity and ρ_f is the density of the nanofluid. $\nu_f = \frac{\mu_f}{\rho_f}$ is the kinematic viscosity, β is the coefficient of volumetric volume expansion of a second grade nanofluid, g is the acceleration due to gravity, C is the nanoparticle volume fraction, $k = k_0x$ is the permeability of porous medium and $k^F = \frac{k_0^F}{\sqrt{x}}$ is the Forchheimer resistance factor where k_0 is the initial permeability. N is the number density of motile microorganisms, C_∞ is the ambient nanofluid volume fraction, $\lambda = \frac{k_1}{\rho_f}$ is the thermal diffusivity of the nanofluid in which k_1 is the thermal conductivity, k_r is the rate (constant) of chemical reaction, $\tau = \frac{(\rho c)_p}{(\rho c)_f}$ is the ratio of nanoparticle heat capacity and the base fluid heat capacity, D_B is the Brownian diffusion coefficient, D_n is the diffusivity of microorganisms, T_∞ is the ambient temperature, D_T is the thermophoretic diffusion coefficient and T is the temperature inside the boundary layer.

The boundary conditions for the nano-bioconvection flow are

$$u = 0, \quad v = 0, \quad -k_1 \frac{\partial T}{\partial y} = h_f(T_f - T), \quad D_B \frac{dC}{dy} + \frac{D_T}{T_\infty} \frac{dT}{dy} = 0, \quad N = N_w \quad \text{at} \quad y = 0, \quad (7)$$

$$u \rightarrow U(x), \quad \frac{\partial u}{\partial y} \rightarrow 0, \quad T \rightarrow T_\infty, \quad C \rightarrow C_\infty, \quad N \rightarrow N_\infty \quad \text{as} \quad y \rightarrow \infty, \quad (8)$$

where $h_f(x)$ denotes the heat transfer coefficient due to T_f , N_w is the wall concentration of microorganisms and N_∞ is the ambient concentration of microorganisms. Note that, in order to satisfy the boundary conditions at infinity, we have to set $N_\infty = 0$.

Introducing the transformations for nondimensional variables f, θ, ϕ, Ω and similarity variable ζ as

$$\psi(x, y) = \left(\frac{4U\nu_f x}{3}\right)^{\frac{1}{2}} f(\zeta), \quad \theta(\zeta) = \frac{T - T_\infty}{T_f - T_\infty}, \quad \phi = \frac{C - C_\infty}{C_w - C_\infty}, \quad \Omega = \frac{N - N_\infty}{N_w - N_\infty}, \quad \zeta = \left[\frac{3U}{4\nu_f x}\right]^{\frac{1}{2}} y, \quad (9)$$

where ψ is the stream function such that $u = \frac{\partial\psi}{\partial y}$ and $v = -\frac{\partial\psi}{\partial x}$, x and y are the Cartesian coordinates along surface and normal to it. Equation (9) automatically satisfies mass conservation Equation (1). With the help of Equation (9), the Equations (2)–(5), (7) and (8) yield the following six Equations (10)–(15).

$$f''' + \frac{2}{3}(1 - f^2) + ff'' + \gamma_1(2ff''' - f'^2 - 3ff''v) + Gr\theta - Nr\phi + Rb\Omega - Mf' - \gamma_3f' - \gamma_4f'^2 = 0, \quad (10)$$

$$\theta'' + Prf\theta' + Nt(\theta')^2 + Nb\theta'\phi' = 0, \quad (11)$$

$$\phi'' + Lef\phi' + \frac{Nt}{Nb}\theta'' - \gamma_5\phi = 0, \quad (12)$$

$$\Omega'' + Scf\Omega' - Pe(\phi'\Omega' + \phi''\Omega) = 0, \quad (13)$$

$$f = f' = 0, \quad \theta' = -\gamma_2(1 - \theta), \quad Nb\phi' + Nt\theta' = 0, \quad \Omega = 1 \quad \text{at} \quad \zeta = 0, \quad (14)$$

$$f' = 1, \quad f'' = 0, \quad \theta = \phi = \Omega = 0 \quad \text{at} \quad \zeta = \infty, \quad (15)$$

where prime (') represents the derivative with respect to ζ and the various parameters in Equations (10)–(14) are explained in Table 2. For $\gamma_1 = 0$, the present study corresponds to viscous nanofluid case and if $\gamma_1 = \gamma_3 = \gamma_4 = \gamma_5 = M = 0$, then the study [14] is recovered.

Table 2. Various parameters in Equations (10)–(14).

Parameter Names	Symbols/Notations	Defined Values
Dimensionless second-grade nanofluid parameter	γ_1	$\frac{\alpha_1 U}{4\mu_f x}$
Thermal Grashof number	Gr	$\frac{2(1 - C_\infty)\rho_f g \beta (T_f - T_\infty)}{3a\rho_f}$
Buoyancy ratio parameter	Nr	$\frac{2(\rho_p - \rho_f)C_\infty g}{3a\rho_f}$
Bioconvection Rayleigh number	Rb	$\frac{2(N_w - N_\infty)g\gamma_{av}\Delta\rho}{3a\rho_f}$
Prandtl number	Pr	$\frac{\nu_f}{\lambda}$
Thermophoresis parameter	Nt	$\frac{\tau D_T (T_f - T_\infty)}{\lambda T_\infty}$
Brownian motion parameter	Nb	$\frac{\tau D_B C_\infty}{\lambda}$
Lewis number	Le	$\frac{\nu_f}{D_B}$
Schmidt number	Sc	$\frac{\nu_f}{D_n}$
Bioconvection Peclet number	Pe	$\frac{bW_c}{D_n}$
Reduced heat transfer parameter	γ_2	$\frac{h_f}{k_1} \sqrt{\frac{4x\nu_f}{3U}}$
Porosity parameter	γ_3	$\frac{4\nu_f}{3k_0 U}$
Inertial parameter	γ_4	$\frac{4k_0^F}{3\sqrt{k_0}}$
Chemical reaction parameter	γ_5	$\frac{4k_r \nu \sqrt{x}}{3bD_B}$
Magnetic field parameter	M	$\frac{4\sigma B_0^2}{3\rho_f U} \sqrt{\frac{x}{2a}}$

3. Entropy Generation

The subject of the present analysis has a close relation with engineering and industrial processes so it is interesting to investigate the rate of entropy generation. The volumetric entropy generation of the fluid can be written as

$$E'''_{gen} = \frac{\lambda}{T_\infty^2} \left(\frac{\partial T}{\partial y}\right)^2 + \frac{\mu}{T_\infty} \left(\frac{\partial u}{\partial y}\right)^2 + \frac{\mu\alpha_1}{T_\infty^2} \left(u \frac{\partial u}{\partial y} \frac{\partial^2 u}{\partial x \partial y} + v \frac{\partial u}{\partial y} \frac{\partial^2 u}{\partial y^2}\right) + \frac{\sigma B_0^2}{T_\infty} u^2 + \frac{RD}{C_\infty} \left(\frac{\partial C}{\partial y}\right)^2 + \frac{RD}{T_\infty} \left[\frac{\partial T}{\partial x} \frac{\partial C}{\partial x} + \frac{\partial T}{\partial y} \frac{\partial C}{\partial y}\right] + \frac{RD}{N_\infty} \left(\frac{\partial N}{\partial y}\right)^2 + \frac{RD}{T_\infty} \left[\frac{\partial T}{\partial x} \frac{\partial N}{\partial x} + \frac{\partial T}{\partial y} \frac{\partial N}{\partial y}\right], \quad (16)$$

where R denotes the ideal gas constant and D represents the diffusivity. In Equation (16), on the right hand side, the first term represents the irreversibility due to heat transfer, the second term is entropy generation due to viscous dissipation, the third term is second grade fluid friction irreversibility, the fourth term is the local entropy generation due to the effect of magnetic field and the fifth to eighth terms are the irreversibilities due to diffusion effect. The characteristic entropy generation rate is

$$E'''_0 = \frac{\lambda(T_f - T_\infty)^2}{L^2 T_\infty^2}, \quad (17)$$

where L is the characteristic length. The entropy generation E_G is the ratio between the entropy generation rate E'''_{gen} and the characteristic entropy generation rate E'''_0 i.e.,

$$E_G = \frac{E_{gen}'''}{E_0'''} \tag{18}$$

Applying Equation (9), the non-dimensional form of Equation (18) for entropy generation number $N_G(\zeta)$ is

$$N_G(\zeta) = Re(\theta')^2 + \frac{ReBr}{(\theta_w)^2} [(f')^2] + \frac{ReBr\gamma_1}{(\theta_w)^2} (f(f'')^2 - 3f'f''f''') + \frac{ReBrM}{(\theta_w)^2} [(f')^2] + Re\gamma_6 \left(\frac{\phi_w}{\theta_w}\right)^2 (\phi')^2 + Re\gamma_6(\gamma_7 + 1) \left(\frac{\phi_w}{\theta_w}\right) \theta' \phi' + Re\gamma_8 \left(\frac{\Omega_w}{\theta_w}\right)^2 (\Omega')^2 + Re\gamma_8(\gamma_7 + 1) \left(\frac{\Omega_w}{\theta_w}\right) \theta' \Omega', \tag{19}$$

where $Re = L^2 \frac{3U}{4\nu_f} x^{-\frac{1}{4}}$ is the Reynolds number, $Br = \frac{\mu U^2}{\lambda T_\infty}$ is the Brinkman number, $\gamma_6 = \frac{RDC_\infty}{\lambda}$ is the diffusive constant parameter due to nanoparticles concentration, $\gamma_7 = \left(\frac{y}{4x}\right)^2$ is nondimensional positive number, $\gamma_8 = \frac{RDN_\infty}{\lambda}$ is the diffusive constant parameter due to gyrotactic microorganisms concentration, $\theta_w = \frac{T_f - T_w}{T_\infty}$, $\phi_w = \frac{C_w - C_\infty}{C_\infty}$ and $\Omega_w = \frac{N_w - N_\infty}{N_\infty}$ are respectively the temperature, nanoparticles concentration and microorganisms concentration differences. Due to entropy generation rate, the second-grade nanofluid parameter and magnetic field parameter, here become respectively $\gamma_1 = \frac{\alpha_1 U}{4T_\infty x}$ and $M = \frac{4\sigma\nu_f B_0^2 x^2}{3\mu_f U^2}$.

4. Analytical Solution of the Problem by Homotopy Analysis Method

The initial approximations and the auxiliary linear operators for velocity, temperature, nanoparticles concentration and motile microorganism concentration are presented as

$$f_0(\zeta) = \zeta - [\exp(-\zeta) - \exp(-2\zeta)], \quad \theta_0(\zeta) = \exp(-\zeta) - \frac{\exp(-2\zeta)}{2+\gamma_2}, \tag{20}$$

$$\phi_0(\zeta) = -\frac{Nt\gamma_2}{Nb(\gamma_2+2)} \exp(-\zeta), \quad \Omega_0(\zeta) = \exp(-\zeta),$$

$$L_f = f''' - f', \quad L_\theta = \theta'' - \theta, \quad L_\phi = \phi'' - \phi, \quad L_\Omega = \Omega'' - \Omega \tag{21}$$

The following properties are related to the linear operators

$$L_f [C_1 + C_2 \exp(\zeta) + C_3 \exp(-\zeta)] = 0, \quad L_\theta [C_4 \exp(\zeta) + C_5 \exp(-\zeta)] = 0, \tag{22}$$

$$L_\phi [C_6 \exp(\zeta) + C_7 \exp(-\zeta)] = 0, \quad L_\Omega [C_8 \exp(\zeta) + C_9 \exp(-\zeta)] = 0,$$

where $C_i(i = 1-9)$ are the arbitrary constants.

4.1. Zeroth-Order Deformation Problems

Introducing the nonlinear operator \aleph as

$$\aleph_f[f(\zeta, p), \theta(\zeta, p), \phi(\zeta, p), \Omega(\zeta, p)] = \frac{\partial^3 f(\zeta, p)}{\partial \zeta^3} + \frac{2}{3} \left[1 - \left(\frac{\partial f(\zeta, p)}{\partial \zeta} \right)^2 \right] + f(\zeta, p) \frac{\partial^2 f(\zeta, p)}{\partial \zeta^2} + \gamma_1 \left[2 \frac{\partial f(\zeta, p)}{\partial \zeta} \frac{\partial^3 f(\zeta, p)}{\partial \zeta^3} - \left(\frac{\partial^2 f(\zeta, p)}{\partial \zeta^2} \right)^2 - 3f(\zeta, p) \frac{\partial^4 f(\zeta, p)}{\partial \zeta^4} \right] + Gr\theta(\zeta, p) - Nr\phi(\zeta, p) + Rb\Omega(\zeta, p) - M \frac{\partial f(\zeta, p)}{\partial \zeta} - \gamma_3 \frac{\partial f(\zeta, p)}{\partial \zeta} - \gamma_4 \left(\frac{\partial f(\zeta, p)}{\partial \zeta} \right)^2, \tag{23}$$

$$\aleph_\theta[f(\zeta, p), \theta(\zeta, p), \phi(\zeta, p)] = \frac{\partial^2 \theta(\zeta, p)}{\partial \zeta^2} + Prf(\zeta, p) \frac{\partial \theta(\zeta, p)}{\partial \zeta} + Nt \left(\frac{\partial \theta(\zeta, p)}{\partial \zeta} \right)^2 + Nb \frac{\partial \theta(\zeta, p)}{\partial \zeta} \frac{\partial \phi(\zeta, p)}{\partial \zeta}, \tag{24}$$

$$\aleph_\phi[f(\zeta, p), \theta(\zeta, p), \phi(\zeta, p)] = \frac{\partial^2 \phi(\zeta, p)}{\partial \zeta^2} + Lef(\zeta, p) \frac{\partial \phi(\zeta, p)}{\partial \zeta} + \frac{Nt}{Nb} \frac{\partial^2 \theta(\zeta, p)}{\partial \zeta^2} - \gamma_5 \phi(\zeta, p), \tag{25}$$

$$\aleph_\Omega[f(\zeta, p), \phi(\zeta, p), \Omega(\zeta, p)] = \frac{\partial^2 \Omega(\zeta, p)}{\partial \zeta^2} + Scf(\zeta, p) \frac{\partial \Omega(\zeta, p)}{\partial \zeta} - Pe \left[\frac{\partial \phi(\zeta, p)}{\partial \zeta} \frac{\partial \Omega(\zeta, p)}{\partial \zeta} + \frac{\partial^2 \phi(\zeta, p)}{\partial \zeta^2} \Omega(\zeta, p) \right], \tag{26}$$

where p is an embedding parameter such that $p \in [0, 1]$.

The zeroth-order deformation problems are expressed as

$$(1 - p)L_f[f(\zeta, p) - f_0(\zeta)] = ph\aleph_f[f(\zeta, p), \theta(\zeta, p), \phi(\zeta, p), \Omega(\zeta, p)], \tag{27}$$

$$(1 - p)L_\theta[\theta(\zeta, p) - \theta_0(\zeta)] = ph\aleph_\theta[f(\zeta, p), \theta(\zeta, p), \phi(\zeta, p)], \tag{28}$$

$$(1 - p)L_\phi[\phi(\zeta, p) - \phi_0(\zeta)] = ph\aleph_\phi[f(\zeta, p), \theta(\zeta, p), \phi(\zeta, p)], \tag{29}$$

$$(1 - p)L_\Omega[\Omega(\zeta, p) - \Omega_0(\zeta)] = ph\aleph_\Omega[f(\zeta, p), \phi(\zeta, p), \Omega(\zeta, p)], \tag{30}$$

where h represents the auxiliary non-zero parameter.

Equations (27)–(30) have the boundary conditions in Equations (31)–(34) respectively

$$f(0, p) = 0, \quad f'(0, p) = 0, \quad f'(\infty, p) = 1. \tag{31}$$

$$\theta'(0, p) = -\gamma_2(1 - \theta(0, p)), \quad \theta(\infty, p) = 0. \tag{32}$$

$$Nb\phi'(0, p) + Nt\theta'(0, p) = 0, \quad \phi(\infty, p) = 0. \tag{33}$$

$$\Omega(0, p) = 1, \quad \Omega(\infty, p) = 0. \tag{34}$$

Assuming $p = 0$ and $p = 1$, the following results hold

$$p = 0 \Rightarrow f(\zeta, 0) = f_0(\zeta) \quad \text{and} \quad p = 1 \Rightarrow f(\zeta, 1) = f(\zeta), \tag{35}$$

$$p = 0 \Rightarrow \theta(\zeta, 0) = \theta_0(\zeta) \quad \text{and} \quad p = 1 \Rightarrow \theta(\zeta, 1) = \theta(\zeta), \tag{36}$$

$$p = 0 \Rightarrow \phi(\zeta, 0) = \phi_0(\zeta) \quad \text{and} \quad p = 1 \Rightarrow \phi(\zeta, 1) = \phi(\zeta), \tag{37}$$

Similarly

$$p = 0 \Rightarrow \Omega(\zeta, 0) = \Omega_0(\zeta) \quad \text{and} \quad p = 1 \Rightarrow \Omega(\zeta, 1) = \Omega(\zeta). \tag{38}$$

Using Taylor series expansion and Equations (27)–(30), gives the following results

$$f(\zeta, p) = f_0(\zeta) + \sum_{m=1}^{\infty} f_m(\zeta)p^m, \quad f_m(\zeta) = \frac{1}{m!} \frac{\partial^m f(\zeta, p)}{\partial p^m} \Big|_{p=0}, \tag{39}$$

$$\theta(\zeta, p) = \theta_0(\zeta) + \sum_{m=1}^{\infty} \theta_m(\zeta)p^m, \quad \theta_m(\zeta) = \frac{1}{m!} \frac{\partial^m \theta(\zeta, p)}{\partial p^m} \Big|_{p=0}, \tag{40}$$

$$\phi(\zeta, p) = \phi_0(\zeta) + \sum_{m=1}^{\infty} \phi_m(\zeta)p^m, \quad \phi_m(\zeta) = \frac{1}{m!} \frac{\partial^m \phi(\zeta, p)}{\partial p^m} \Big|_{p=0}, \tag{41}$$

$$\Omega(\zeta, p) = \Omega_0(\zeta) + \sum_{m=1}^{\infty} \Omega_m(\zeta)p^m, \quad \Omega_m(\zeta) = \frac{1}{m!} \frac{\partial^m \Omega(\zeta, p)}{\partial p^m} \Big|_{p=0}. \tag{42}$$

The convergence of the series is closely related to h . The value of h is taken in such a way that the series in Equations (39)–(42) converge at $p = 1$, then Equations (39)–(42) result in

$$f(\zeta) = f_0(\zeta) + \sum_{m=1}^{\infty} f_m(\zeta), \tag{43}$$

$$\theta(\zeta) = \theta_0(\zeta) + \sum_{m=1}^{\infty} \theta_m(\zeta), \tag{44}$$

$$\phi(\zeta) = \phi_0(\zeta) + \sum_{m=1}^{\infty} \phi_m(\zeta), \tag{45}$$

$$\Omega(\zeta) = \Omega_0(\zeta) + \sum_{m=1}^{\infty} \Omega_m(\zeta). \tag{46}$$

4.2. m -th Order Deformation Problems

By taking m times derivative with respect to p of Equations ((27), (31)), ((28), (32)), ((29), (33)) and ((30), (34)), then dividing by $m!$ and substituting $p = 0$ in each computation, yield the following m -th order deformation problems

$$L_f[f_m(\zeta) - \chi_m f_{m-1}(\zeta)] = hR_m^f(\zeta), \tag{47}$$

$$f_m(0) = f'_m(0) = f'_m(\infty) = 0, \tag{48}$$

$$R_m^f(\zeta) = f'''_{m-1} + \frac{2}{3} \sum_{k=0}^{m-1} [1 - f'_{m-1-k} f'_k] + \sum_{k=0}^{m-1} [f_{m-1-k} f''_k] + \gamma_1 \sum_{k=0}^{m-1} [2f'_{m-1-k} f'''_k - f''_{m-1-k} f''_k - 3f_{m-1-k} f_k^{iv}] + Gr\theta_{m-1} - Nr\phi_{m-1} + Rb\Omega_{m-1} - Mf'_{m-1} - \gamma_3 f'_{m-1} - \gamma_4 \sum_{k=0}^{m-1} f'_{m-1-k} f'_k. \tag{49}$$

$$L_\theta[\theta_m(\zeta) - \chi_m \theta_{m-1}(\zeta)] = hR_m^\theta(\zeta), \tag{50}$$

$$\theta'_m(0) = \theta_m(\infty) = 0, \tag{51}$$

$$R_m^\theta(\zeta) = \theta''_{m-1} + Pr \sum_{k=0}^{m-1} f_{m-1-k} \theta'_k + Nt \sum_{k=0}^{m-1} \theta'_{m-1-k} \theta'_k + Nb \sum_{k=0}^{m-1} \theta'_{m-1-k} \phi'_k. \tag{52}$$

$$L_\phi[\phi_m(\zeta) - \chi_m \phi_{m-1}(\zeta)] = hR_m^\phi(\zeta), \tag{53}$$

$$Nb\phi'_m(0) + Nt\theta'_m(0) = \phi_m(\infty) = 0, \tag{54}$$

$$R_m^\phi(\zeta) = \phi''_{m-1} + Le \sum_{k=0}^{m-1} f_{m-1-k} \phi'_k + \frac{Nt}{Nb} \theta''_{m-1} - \gamma_5 \phi_{m-1}. \tag{55}$$

$$L_\Omega[\Omega_m(\zeta) - \chi_m \Omega_{m-1}(\zeta)] = hR_m^\Omega(\zeta), \tag{56}$$

$$\Omega_m(0) = \Omega'_m(\infty) = 0, \tag{57}$$

$$R_m^\Omega(\zeta) = \Omega''_{m-1} + Sc \sum_{k=0}^{m-1} f_{m-1-k} \Omega'_k - Pe \sum_{k=0}^{m-1} [\phi'_{m-1-k} \Omega'_k + \phi''_{m-1-k} \Omega_k], \tag{58}$$

$$\chi_m = \begin{cases} 0, & m \leq 1 \\ 1, & m > 1. \end{cases} \tag{59}$$

If $f_m^*(\zeta)$, $\theta_m^*(\zeta)$, $\phi_m^*(\zeta)$ and $\Omega_m^*(\zeta)$ are the particular solutions, then the general solutions of Equations (47), (50), (54) and (56) are

$$f_m(\zeta) = f_m^*(\zeta) + C_1 + C_2 \exp(\zeta) + C_3 \exp(-\zeta), \tag{60}$$

$$\theta_m(\zeta) = \theta_m^*(\zeta) + C_4 \exp(\zeta) + C_5 \exp(-\zeta), \tag{61}$$

$$\phi_m(\zeta) = \phi_m^*(\zeta) + C_6 \exp(\zeta) + C_7 \exp(-\zeta), \tag{62}$$

$$\Omega_m(\zeta) = \Omega_m^*(\zeta) + C_8 \exp(\zeta) + C_9 \exp(-\zeta). \tag{63}$$

5. Results

The non-linear differential Equations (10)–(13) with boundary conditions in Equations (14) and (15) have been solved with the help of symbolic computation software MATHEMATICA employing HAM program. The effects of embedded parameters on the velocity $f(\zeta)$, temperature $\theta(\zeta)$, concentration $\phi(\zeta)$, motile gyrotactic microorganisms $\Omega(\zeta)$ fields and entropy generation have been plotted in Figures 6–17, 8–25, 26–35 and 36–46 respectively. Similarly the residual error graphs have been shown in Figures 54–57. The schematic illustration of the problem is seen in Figure 1. Liao [27] introduced h curves for the convergence of the series solutions of the problems. Therefore, the admissible h -curves for $f(\zeta)$, $\theta(\zeta)$, $\phi(\zeta)$ and $\Omega(\zeta)$ are drawn in the ranges $-1.3 \leq h \leq 0.0$, $-1.8 \leq h \leq 0.2$, $-2.1 \leq h \leq 0.1$ and $-2.0 \leq h \leq 0.0$ in Figures 2–5.

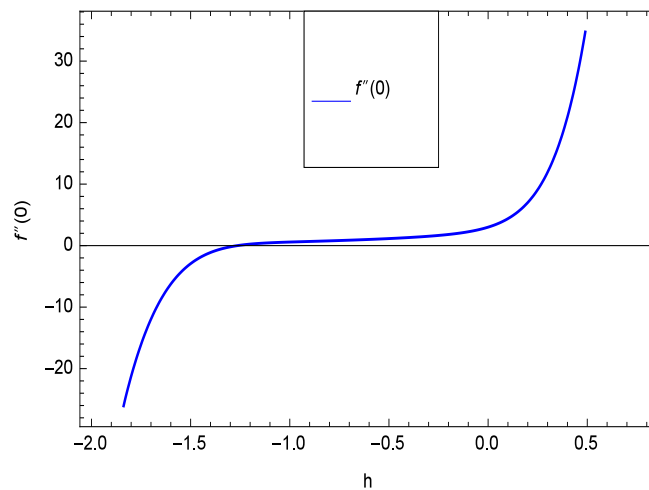


Figure 2. The h curve of $f(\zeta)$.

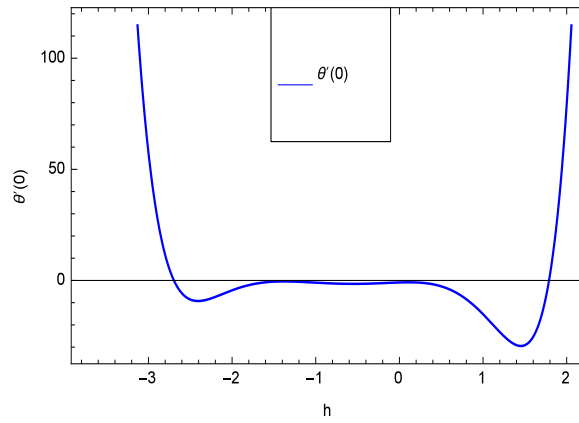


Figure 3. The h curve of $\theta(\zeta)$.

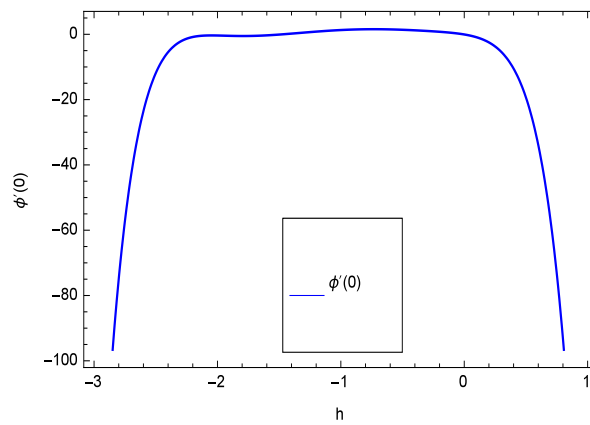


Figure 4. The h curve of $\phi(\zeta)$.

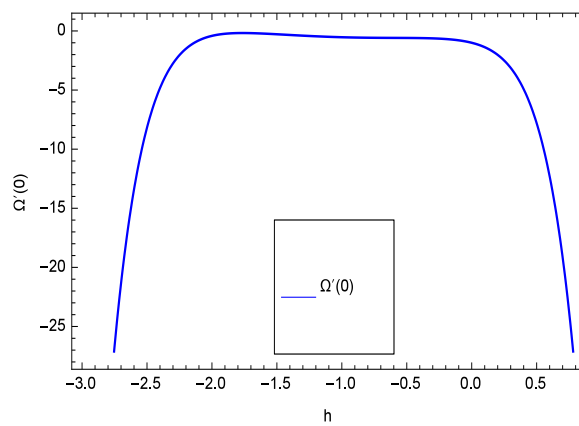


Figure 5. The h curve of $\Omega(\zeta)$.

6. Discussion

6.1. Velocity Profile

This section depicts the influence of numerous dimensionless parameters on the velocity $f(\zeta)$. Figure 6 shows that the velocity profile decreases significantly with an enhancement in the values of second grade nanofluid parameter γ_1 . Velocity is minimum for non-Newtonian nanofluids in general. Figure 7 demonstrates that the non-dimensional velocity profile $f(\zeta)$ increases for the greater values of reduced heat transfer parameter γ_2 due to slip condition. Figure 8 reveals that the non-dimensional velocity profile $f(\zeta)$ depreciates for the high values of porosity parameter γ_3 . The holes of the medium creates resistance to the flow thereby decreasing the motion. Figure 9 is prepared for the inertial parameter γ_4 . An increment in this parameter decreases the velocity $f(\zeta)$. In Figure 10, it is seen that the non-dimensional velocity $f(\zeta)$ amplifies with increasing magnitude of chemical reaction parameter γ_5 which shows that velocity enhances with the strengthening of chemical reaction. Figure 11 shows that the non-dimensional velocity $f(\zeta)$ increases with the increasing magnitude of buoyancy parameter Gr . Gravitational force favors the second grade nanofluid flow along the vertical solid surface. The buoyancy ratio parameter Nr is showing its effect in Figure 12. An enhancement in the parameter Nr makes a sharp advancement in the nanofluid flow so velocity $f(\zeta)$ becomes high. In Figure 13, the velocity $f(\zeta)$ decreases for increasing quantities of bioconvection Rayleigh number Rb which characterizes the effect of up-swimming of microorganisms. It should be noted that there is no effect of Rb on the boundary layer thickness. For the case of pure natural convection, $Rb = 0$ which implies that microorganisms have the same density as water and, therefore, they do not contribute to density stratification (or which corresponds to the situation with zero concentration of microorganisms). Since the microorganisms swim on average in the upward direction, their presence produces a destabilizing effect and reduces the critical value of Rb . By increasing the average concentration of corresponding microorganisms in the suspension, Rb can be increased. Figure 14 depicts the role of Lewis number Le . Velocity $f(\zeta)$ is found to be maximized with greater values of Le . Nanoparticles concentrations are consistently depressed with greater lewis number; nevertheless the over-riding influence is imposed by the lewis number on the diffusion of nanoparticles. The role of Schmidt number Sc is projected in Figure 15 which shows that velocity $f(\zeta)$ amplifies with the effective diffusion of microorganisms and the acceleration of nanoparticles. Figure 16 demonstrates that the velocity $f(\zeta)$ decelerates with the rising values of magnetic field parameter M . It is due to the fact that the magnetic field exerts a force, known as Lorentz force which suppresses the velocity. Figure 17 illustrates that the velocity $f(\zeta)$ enhances by the high values of the Prandtl number Pr . It is evident that high quantities of Pr make enhancement in the mass transfer rate so $f(\zeta)$ elevates due to gravity.

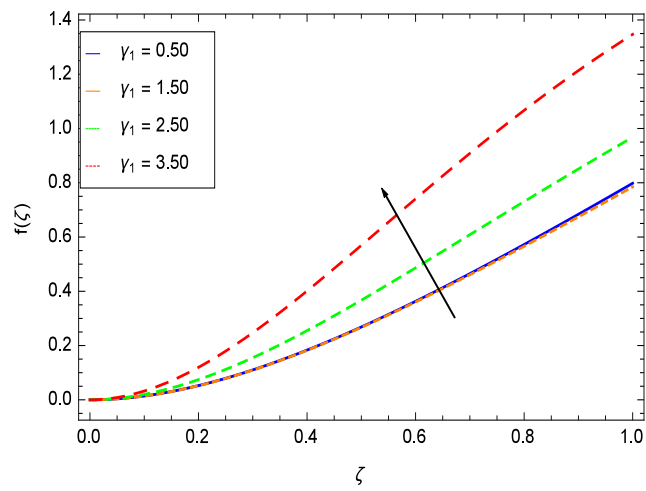


Figure 6. Effect on velocity profile for $h = -1.30$, $\gamma_2 = 0.60$, $\gamma_3 = 0.20$, $\gamma_4 = 0.30$, $\gamma_5 = 1.00$, $Gr = 0.50$, $Nr = 0.60$, $Rb = 0.70$, $Nb = 0.80$, $Nt = 0.90$, $Le = 0.60$, $Sc = 0.70$, $Pe = 1.00$, $M = 1.00$, $Pr = 10.00$ and different values of γ_1 .

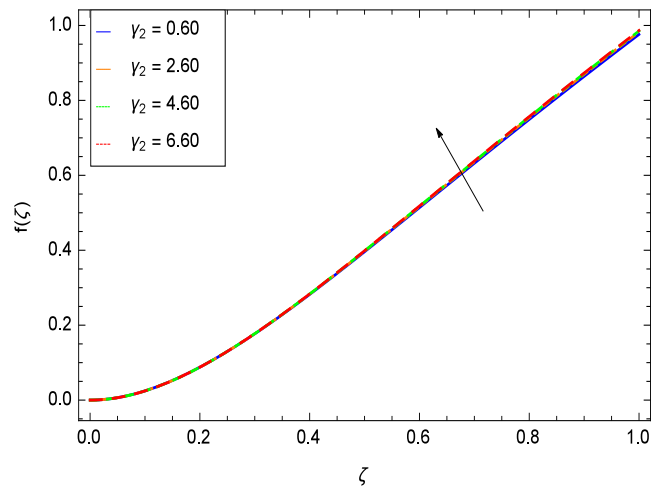


Figure 7. Effect on velocity profile for $h = -1.00$, $\gamma_1 = 0.50$, $\gamma_3 = 0.20$, $\gamma_4 = 0.30$, $\gamma_5 = 1.00$, $Gr = 0.50$, $Nr = 0.60$, $Rb = 0.70$, $Nb = 0.80$, $Nt = 0.90$, $Le = 0.60$, $Sc = 0.70$, $Pe = 1.00$, $M = 1.00$, $Pr = 10.00$ and different values of γ_2 .

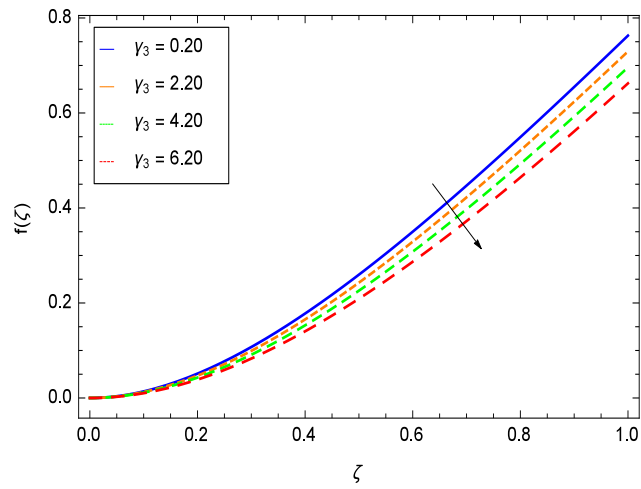


Figure 8. Effect on velocity profile for $h = 0.10$, $\gamma_1 = 0.50$, $\gamma_2 = 0.60$, $\gamma_4 = 0.30$, $\gamma_5 = 1.00$, $Gr = 0.50$, $Nr = 0.60$, $Rb = 0.70$, $Nb = 0.80$, $Nt = 0.90$, $Le = 0.60$, $Sc = 0.70$, $Pe = 1.00$, $M = 1.00$, $Pr = 10.00$ and different values of γ_3 .

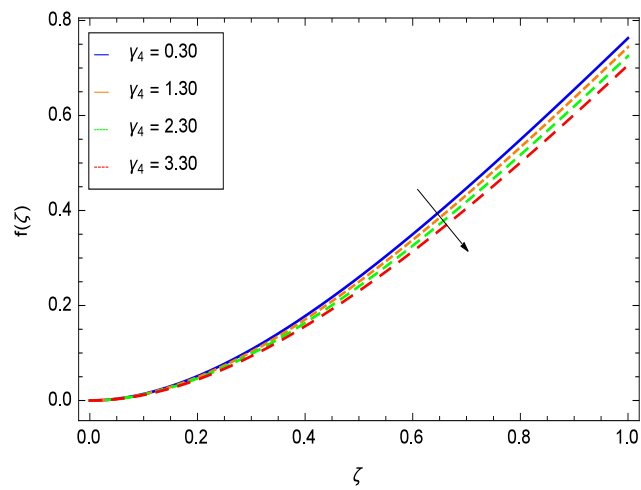


Figure 9. Effect on velocity profile for $h = 0.10$, $\gamma_1 = 0.50$, $\gamma_3 = 0.20$, $\gamma_2 = 0.60$, $\gamma_5 = 1.00$, $Gr = 0.50$, $Nr = 0.60$, $Rb = 0.70$, $Nb = 0.80$, $Nt = 0.90$, $Le = 0.60$, $Sc = 0.70$, $Pe = 1.00$, $M = 1.00$, $Pr = 10.00$ and different values of γ_4 .

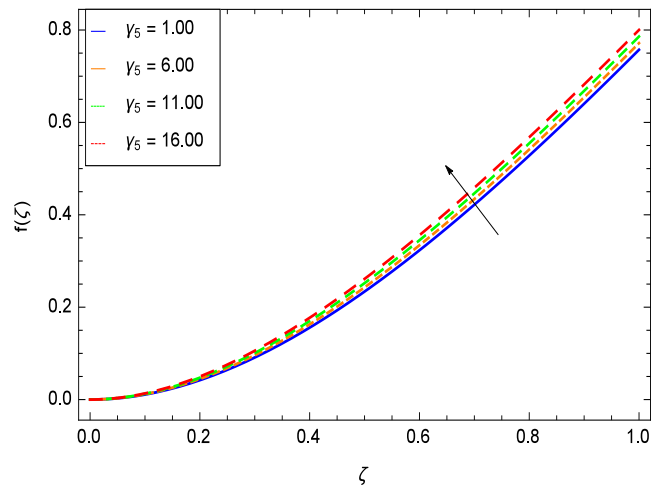


Figure 10. Effect on velocity profile for $h = 0.10$, $\gamma_1 = 0.50$, $\gamma_3 = 0.20$, $\gamma_2 = 0.60$, $\gamma_4 = 0.30$, $Gr = 0.50$, $Nr = 0.60$, $Rb = 0.70$, $Nb = 0.80$, $Nt = 0.90$, $Le = 0.60$, $Sc = 0.70$, $Pe = 1.00$, $M = 1.00$, $Pr = 10.00$ and different values of γ_5 .

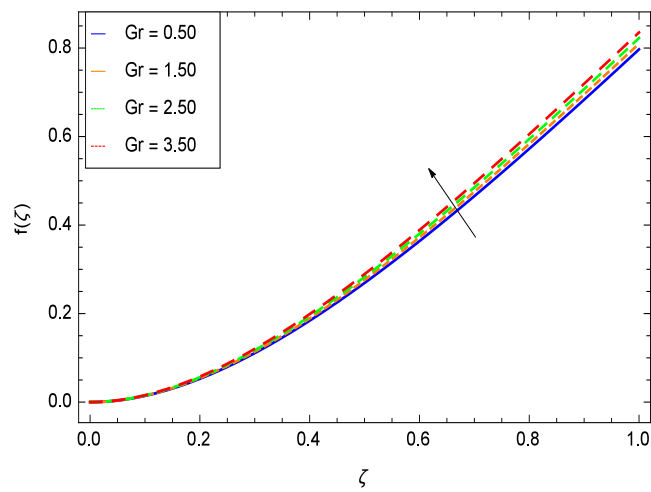


Figure 11. Effect on velocity profile for $h = -1.10$, $\gamma_1 = 0.50$, $\gamma_2 = 0.60$, $\gamma_3 = 0.20$, $\gamma_4 = 0.30$, $\gamma_5 = 1.00$, $Nr = 0.60$, $Rb = 0.70$, $Nb = 0.80$, $Nt = 0.90$, $Le = 0.60$, $Sc = 0.70$, $Pe = 1.00$, $M = 1.00$, $Pr = 10.00$ and different values of Gr .

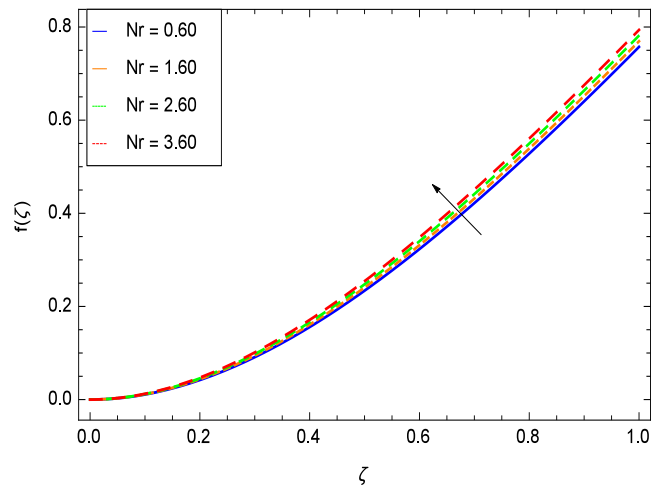


Figure 12. Effect on velocity profile for $h = -3.00$, $\gamma_1 = 0.50$, $\gamma_2 = 0.60$, $\gamma_3 = 0.20$, $\gamma_4 = 0.30$, $\gamma_5 = 1.00$, $Gr = 0.50$, $Rb = 0.70$, $Nb = 0.80$, $Nt = 0.90$, $Le = 0.60$, $Sc = 0.70$, $Pe = 1.00$, $M = 1.00$, $Pr = 10.00$ and different values of Nr .

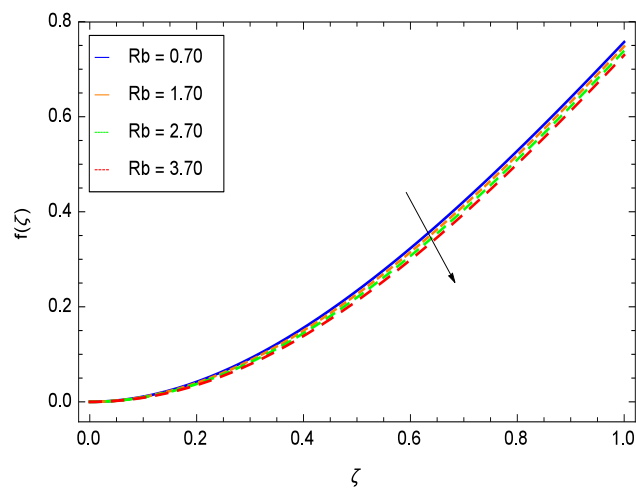


Figure 13. Effect on velocity profile for $h = -3.00$, $\gamma_1 = 0.50$, $\gamma_2 = 0.60$, $\gamma_3 = 0.20$, $\gamma_4 = 0.30$, $\gamma_5 = 1.00$, $Gr = 0.50$, $Nr = 0.60$, $Nb = 0.80$, $Nt = 0.90$, $Le = 0.60$, $Sc = 0.70$, $Pe = 1.00$, $M = 1.00$, $Pr = 10.00$ and different values of Rb .

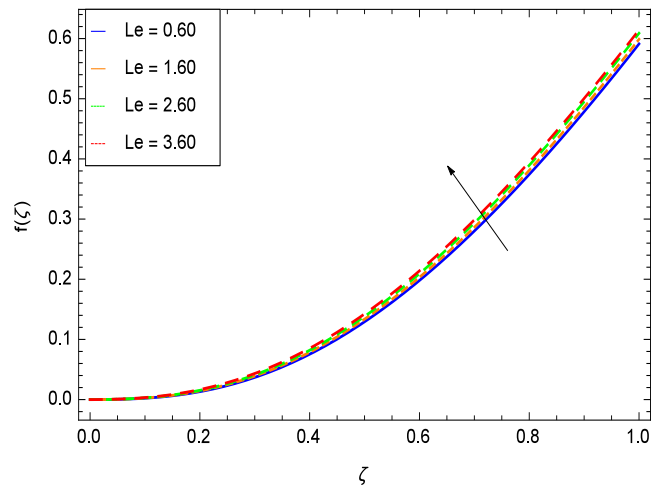


Figure 14. Effect on velocity profile for $h = -5.00$, $\gamma_1 = 0.50$, $\gamma_2 = 0.60$, $\gamma_3 = 0.20$, $\gamma_4 = 0.30$, $\gamma_5 = 1.00$, $Gr = 0.50$, $Rb = 0.70$, $Nb = 0.80$, $Nt = 0.90$, $Nr = 0.60$, $Sc = 0.70$, $Pe = 1.00$, $M = 1.00$, $Pr = 10.00$ and different values of Le .

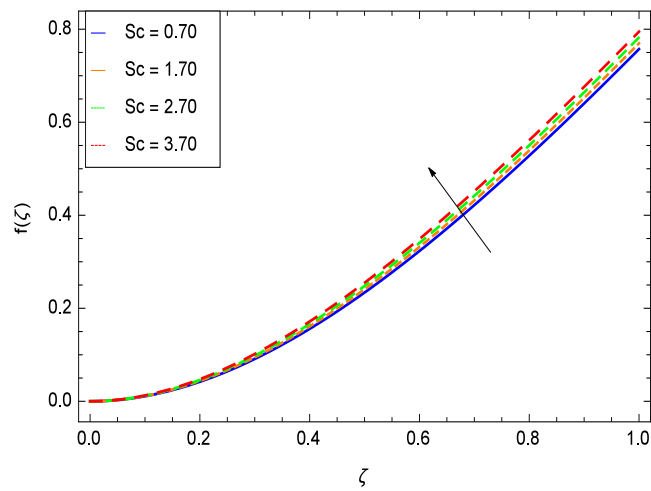


Figure 15. Effect on velocity profile for $h = -3.00$, $\gamma_1 = 0.50$, $\gamma_2 = 0.60$, $\gamma_3 = 0.20$, $\gamma_4 = 0.30$, $\gamma_5 = 1.00$, $Gr = 0.50$, $Rb = 0.70$, $Nb = 0.80$, $Nt = 0.90$, $Le = 0.60$, $Nr = 0.60$, $Pe = 1.00$, $M = 1.00$, $Pr = 10.00$ and different values of Sc .

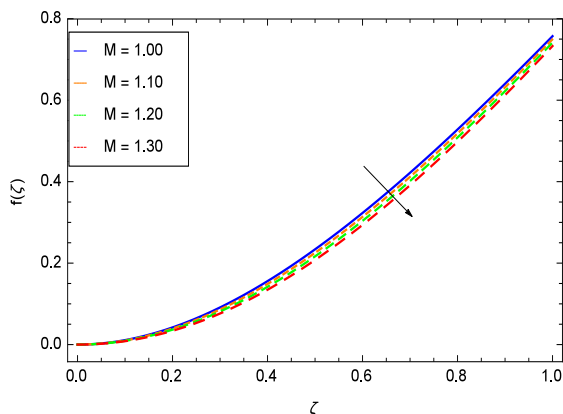


Figure 16. Effect on velocity profile for $h = -3.00, \gamma_1 = 0.50, \gamma_2 = 0.60, \gamma_3 = 0.20, \gamma_4 = 0.30, \gamma_5 = 1.00, Gr = 0.50, Rb = 0.70, Nb = 0.80, Nt = 0.90, Le = 0.60, Nr = 0.60, Pe = 1.00, Pr = 10.00$ and different values of M .

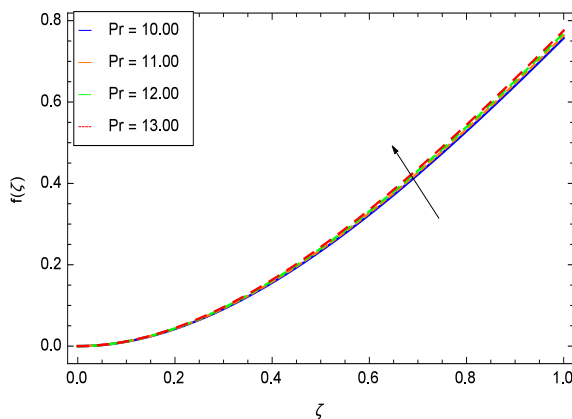


Figure 17. Effect on velocity profile for $h = -3.00, \gamma_1 = 0.50, \gamma_2 = 0.60, \gamma_3 = 0.20, \gamma_4 = 0.30, \gamma_5 = 1.00, Gr = 0.50, Rb = 0.70, Nb = 0.80, Nt = 0.90, Le = 0.60, Sc = 0.70, Pe = 1.00, Nr = 0.60, M = 1.00$ and different values of Pr .

6.2. Temperature Profile

Temperature profile exhibits the interesting behavior for various parameters. Figure 18 shows the influence of second grade nanofluid parameter γ_1 . It demonstrates that the temperature $\theta(\zeta)$ increases with the non-Newtonian effect of the nanofluid. The thermal slip effect is led by reduced heat transfer parameter γ_2 and is exhibited in Figure 19. The graph projects that with the elevation of reduced heat transfer parameter γ_2 , temperature $\theta(\zeta)$ diminishes consequently the decrement comes into play in the thermal boundary layer thickness. Figure 20 reveals that as the porosity parameter γ_3 increases, the surface area of the porous media increases which drops down the temperature. Figure 21 depicts that as the values of inertial parameter γ_4 increases, the temperature diminishes in the boundary region. Figure 22 clearly shows that temperature increases with increasing chemical reaction parameter γ_5 . It is seen that temperature $\theta(\zeta)$ increases with the sharpness of chemical reaction. Indeed, some chemical reactions like fissions and fusions make the temperature high. The thermophoresis parameter Nt gives rise in temperature with larger values of Nt as demonstrated by Figure 23. The thermophoresis parameter Nt is directly proportional to the heat transfer associated with the hot nanofluid. Thus an increment in the thermophoresis parameter Nt causes reduction in the heat transfer at the surface, consequently the

temperature at the surface of the plate increases. Physically, it is due to the fact that with an enhancement of the thermophoresis parameter Nt , the random motion of the particles increases, resulting in an increase in the temperature profile. Due to the Brownian motion, the particles are much closer and so enhance the heat flow among the particles. Figure 24 depicts that the nondimensional temperature $\theta(\zeta)$ decreases for the increasing values of magnetic field parameter M . It is due to the gravity because temperature rises at height and it falls down in tending towards ground. The influence of Prandtl number Pr has been projected in Figure 25 showing that the temperature $\theta(\zeta)$ diminishes with the increasing values of Pr . The reason is that the increasing values of Prandtl number increase the viscosity of the fluid which absorbs the heat as a result, cooling phenomenon is generated.

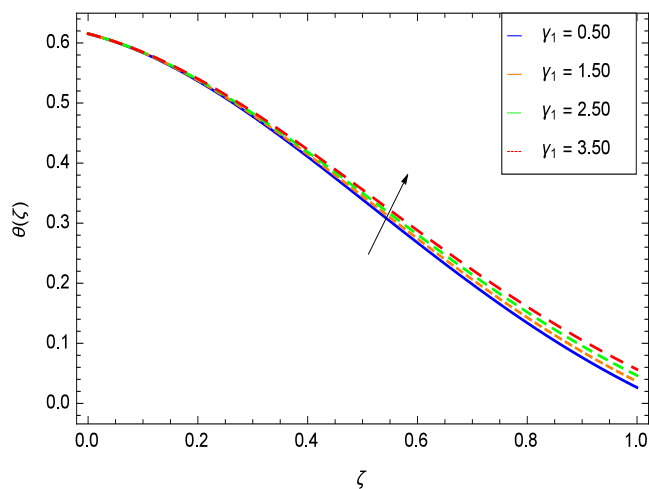


Figure 18. Effect on temperature profile for $h = -0.80, \gamma_2 = 0.60, \gamma_3 = 0.20, \gamma_4 = 0.30, \gamma_5 = 1.00, Gr = 0.50, Nr = 0.60, Rb = 0.70, Nb = 0.80, Nt = 0.90, Le = 0.60, Sc = 0.70, Pe = 1.00, M = 1.00, Pr = 10.00$ and different values of γ_1 .

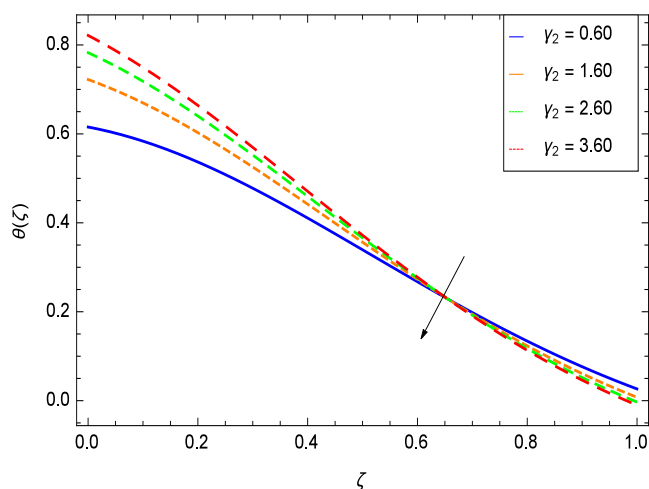


Figure 19. Effect on temperature profile for $h = -0.80, \gamma_1 = 0.50, \gamma_3 = 0.20, \gamma_4 = 0.30, \gamma_5 = 1.00, Gr = 0.50, Nr = 0.60, Rb = 0.70, Nb = 0.80, Nt = 0.90, Le = 0.60, Sc = 0.70, Pe = 1.00, M = 1.00, Pr = 10.00$ and different values of γ_2 .

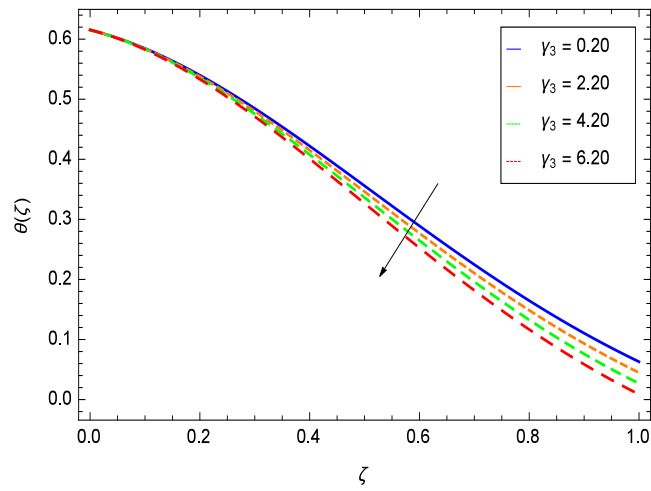


Figure 20. Effect on temperature profile for $h = -0.80$, $\gamma_1 = 0.50$, $\gamma_2 = 0.60$, $\gamma_4 = 0.30$, $\gamma_5 = 1.00$, $Gr = 0.50$, $Nr = 0.60$, $Rb = 0.70$, $Nb = 0.80$, $Nt = 0.90$, $Le = 0.60$, $Sc = 0.70$, $Pe = 1.00$, $M = 1.00$, $Pr = 10.00$ and different values of γ_3 .

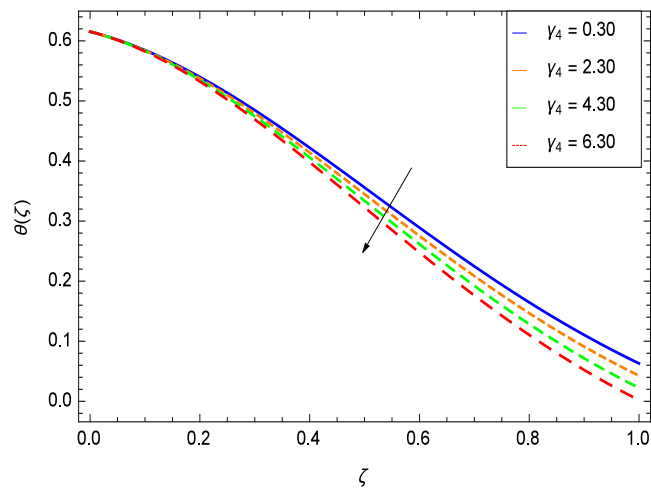


Figure 21. Effect on temperature profile for $h = -0.80$, $\gamma_1 = 0.50$, $\gamma_3 = 0.20$, $\gamma_2 = 0.60$, $\gamma_5 = 1.00$, $Gr = 0.50$, $Nr = 0.60$, $Rb = 0.70$, $Nb = 0.80$, $Nt = 0.90$, $Le = 0.60$, $Sc = 0.70$, $Pe = 1.00$, $M = 1.00$, $Pr = 10.00$ and different values of γ_4 .

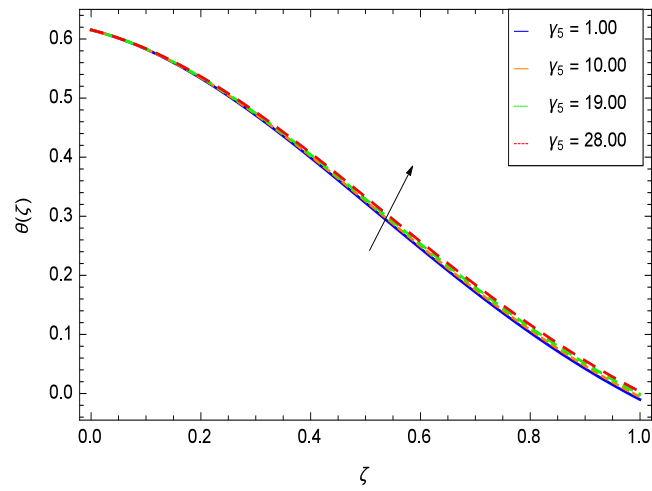


Figure 22. Effect on temperature profile for $h = -0.90$, $\gamma_1 = 0.50$, $\gamma_3 = 0.20$, $\gamma_2 = 0.60$, $\gamma_4 = 0.30$, $Gr = 0.50$, $Nr = 0.60$, $Rb = 0.70$, $Nb = 0.80$, $Nt = 0.90$, $Le = 0.60$, $Sc = 0.70$, $Pe = 1.00$, $M = 1.00$, $Pr = 10.00$ and different values of γ_5 .

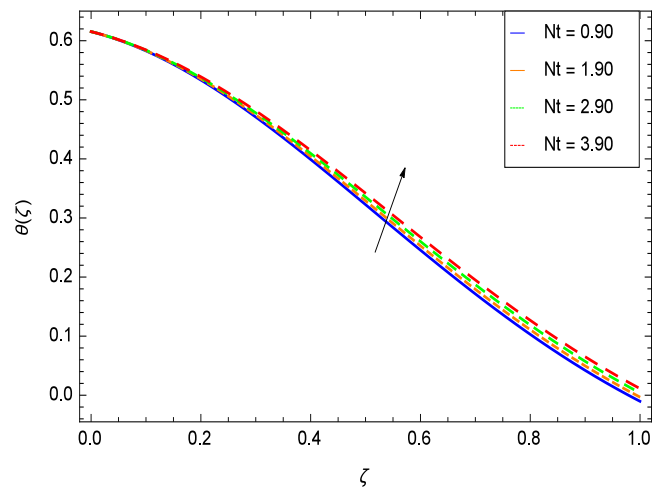


Figure 23. Effect on temperature profile for $h = -0.90$, $\gamma_1 = 0.50$, $\gamma_2 = 0.60$, $\gamma_3 = 0.20$, $\gamma_4 = 0.30$, $\gamma_5 = 1.00$, $Nr = 0.60$, $Rb = 0.70$, $Nb = 0.80$, $Gr = 0.50$, $Le = 0.60$, $Sc = 0.70$, $Pe = 1.00$, $M = 1.00$, $Pr = 10.00$ and different values of Nt .

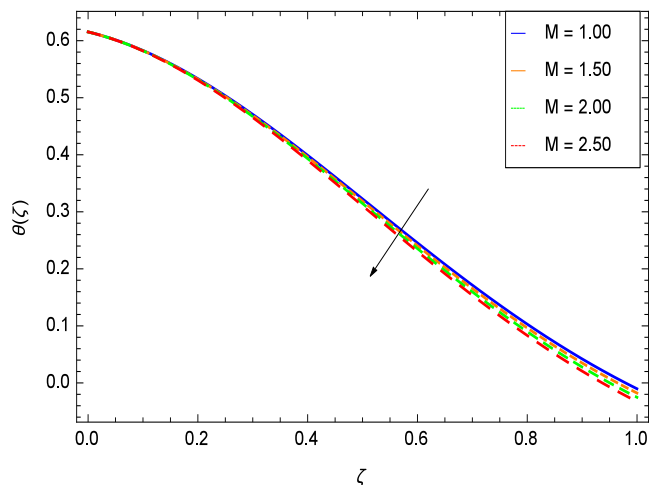


Figure 24. Effect on temperature profile for $h = -0.50, \gamma_1 = 0.50, \gamma_2 = 0.60, \gamma_3 = 0.20, \gamma_4 = 0.30, \gamma_5 = 1.00, Nr = 0.60, Rb = 0.70, Nb = 0.80, Nt = 0.90, Gr = 0.50, Sc = 0.70, Pe = 1.00, Pr = 10.00$ and different values of M .

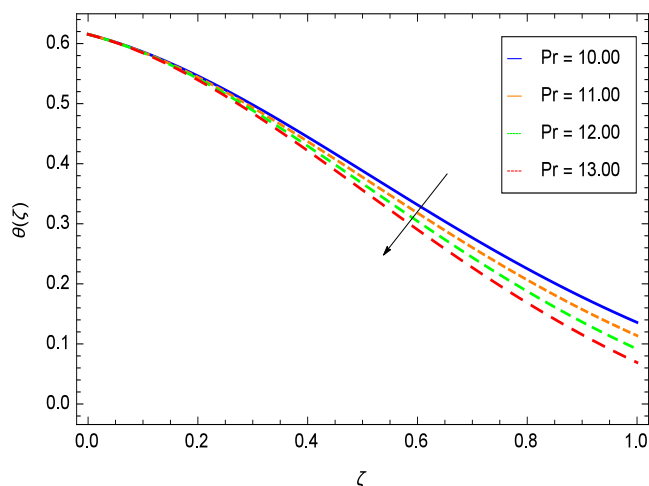


Figure 25. Effect on temperature profile for $h = -0.50, \gamma_1 = 0.50, \gamma_2 = 0.60, \gamma_3 = 0.20, \gamma_4 = 0.30, \gamma_5 = 1.00, Nr = 0.60, Rb = 0.70, Nb = 0.80, Nt = 0.90, Le = 0.60, Sc = 0.70, Pe = 1.00, Gr = 0.50, M = 1.00$ and different values of Pr .

6.3. Nanoparticle Concentration Profile

Nanoparticles having one or more dimensions of the order 100 nm or less have attracted great attention due to their unusual and fascinating properties and applications. Figure 26 displays that the concentration decreases with the non-Newtonian second grade nanofluid parameter γ_1 . The non-Newtonian second grade nanofluid is saturated so there is less opportunity for the diffusion of the nanoparticles, therefore, the concentration decreases. Figure 27 shows the effect of reduced heat parameter γ_2 on concentration $\phi(\zeta)$. It is a common phenomenon that concentration depreciates with decreasing temperature so in the present case, the concentration $\phi(\zeta)$ falls down with decreasing the reduced heat parameter γ_2 . Figure 28 focuses on the role of porosity parameter γ_3 . It provides that the concentration is enhanced with the rising values of porosity parameter γ_3 . The performance of inertial parameter γ_4 is shown in Figure 29 against the non-dimensional concentration profile $\phi(\zeta)$. Concentration makes development with inertia

since saturation is easily received. The highlights of the impact of chemical reaction parameter γ_5 is revealed in Figure 30. It is reported that for constructive (or generation) chemical reaction, the mass transfer shows an increasing behavior i.e., it is seen that the concentration profile increases significantly for the larger values of the chemical reaction parameter γ_5 . Figure 31 projects the role of Brownian motion parameter Nb . Due to Brownian motion, the random motion of the particles increases, which favors the non-dimensional nanoparticle concentration profile $\phi(\zeta)$. Figure 32 illustrates that by enhancing the thermophoresis parameter Nt , the concentration profile $\phi(\zeta)$ depreciates. The nanoparticle concentration boundary layer thickness is an increasing function of the thermophoresis parameter Nt . This indicates that an increment in the thermophoresis parameter Nt induces resistance to the diffusion of the solute and this assists in the reduction of the concentration gradient at the surface. It is interesting to note that the effect of the thermophoresis parameter is more pronounced for the nanoparticle volume fraction than on the fluid velocity and temperature profiles. Figure 33 is specified for the effect of Lewis number Le on the concentration field $\phi(\zeta)$ which reveals that the concentration becomes rich for the different values of the Lewis number Le . The fact is that the performance of the nanoparticles movement is developed, which enhances the nanoparticles concentration. An increment in the Lewis number Le causes the reduction in the mass diffusivity of the nanofluid which in turn reduces the solute concentration. Figure 34 shows that the nondimensional concentration field $\phi(\zeta)$ increases as the magnetic field parameter M increases. It is due to the existence of Lorentz force which shows resistivity to the over all motion, consequently, nanoparticle concentration increases. The magnetic field parameter increases the friction between nanofluid layers so the concentration boundary layer thickness gets enhanced. The influence of Prandtl number Pr on the nanoparticle concentration profile $\phi(\zeta)$ is depicted in Figure 35. Prandtl number is the fluid viscosity parameter so by increasing Prandtl number, the internal viscous forces of the fluid is strong and the concentration goes to peak which causes no special capability for further nanoparticles concentration. Therefore, concentration $\phi(\zeta)$ becomes weak with larger values of Pr .

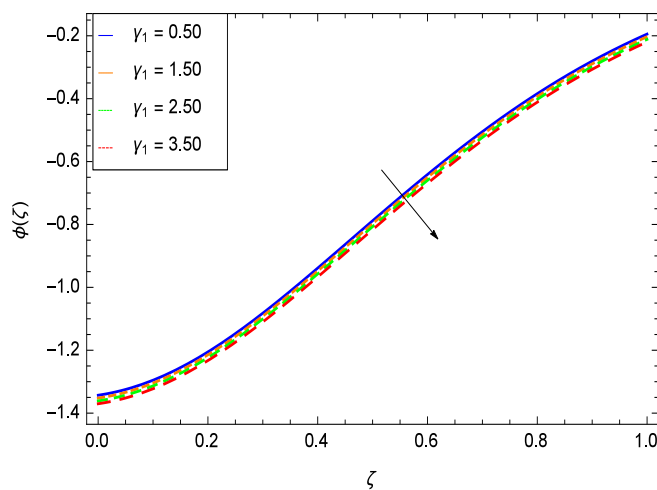


Figure 26. Effect on concentration profile for $h = -3.00$, $\gamma_2 = 0.60$, $\gamma_3 = 0.20$, $\gamma_4 = 0.30$, $\gamma_5 = 1.00$, $Gr = 0.50$, $Nr = 0.60$, $Rb = 0.70$, $Nb = 0.80$, $Nt = 0.90$, $Le = 0.60$, $Sc = 0.70$, $Pe = 1.00$, $M = 1.00$, $Pr = 10.00$ and different values of γ_1 .

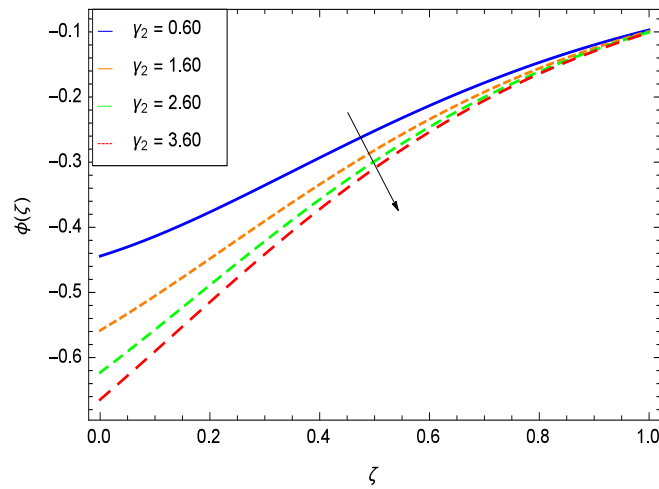


Figure 27. Effect on concentration profile for $h = -3.00$, $\gamma_1 = 0.50$, $\gamma_3 = 0.20$, $\gamma_4 = 0.30$, $\gamma_5 = 1.00$, $Gr = 0.50$, $Nr = 0.60$, $Rb = 0.70$, $Nb = 0.80$, $Nt = 0.90$, $Le = 0.60$, $Sc = 0.70$, $Pe = 1.00$, $M = 1.00$, $Pr = 10.00$ and different values of γ_2 .

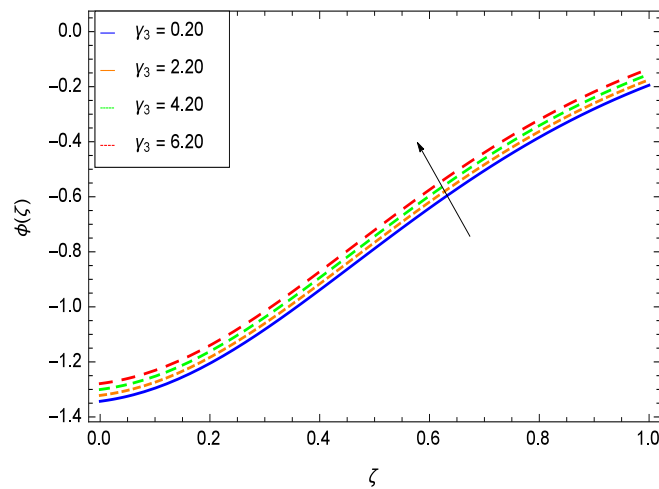


Figure 28. Effect on concentration profile for $h = -3.00$, $\gamma_1 = 0.50$, $\gamma_2 = 0.60$, $\gamma_4 = 0.30$, $\gamma_5 = 1.00$, $Gr = 0.50$, $Nr = 0.60$, $Rb = 0.70$, $Nb = 0.80$, $Nt = 0.90$, $Le = 0.60$, $Sc = 0.70$, $Pe = 1.00$, $M = 1.00$, $Pr = 10.00$ and different values of γ_3 .

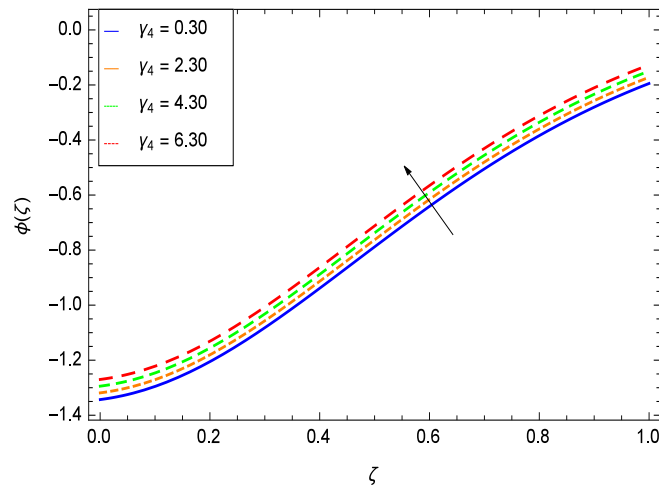


Figure 29. Effect on concentration profile for $h = -3.00$, $\gamma_1 = 0.50$, $\gamma_3 = 0.20$, $\gamma_2 = 0.60$, $\gamma_5 = 1.00$, $Gr = 0.50$, $Nr = 0.60$, $Rb = 0.70$, $Nb = 0.80$, $Nt = 0.90$, $Le = 0.60$, $Sc = 0.70$, $Pe = 1.00$, $M = 1.00$, $Pr = 10.00$ and different values of γ_4 .

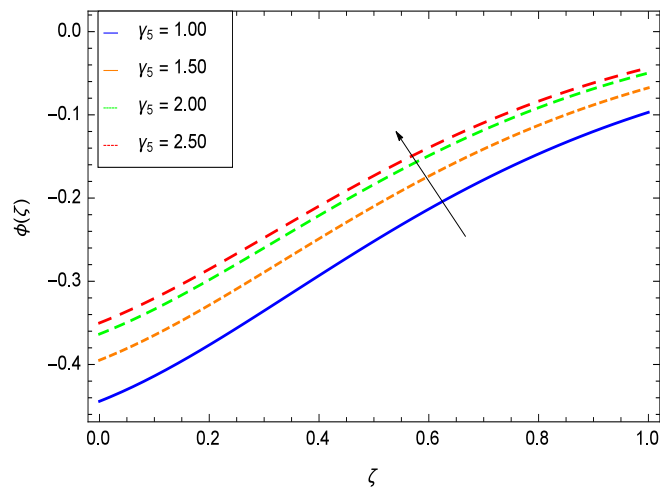


Figure 30. Effect on concentration profile for $h = -1.00$, $\gamma_1 = 0.50$, $\gamma_3 = 0.20$, $\gamma_4 = 0.30$, $\gamma_2 = 0.60$, $Gr = 0.50$, $Nr = 0.60$, $Rb = 0.70$, $Nb = 0.80$, $Nt = 0.90$, $Le = 0.60$, $Sc = 0.70$, $Pe = 1.00$, $M = 1.00$, $Pr = 10.00$ and different values of γ_5 .

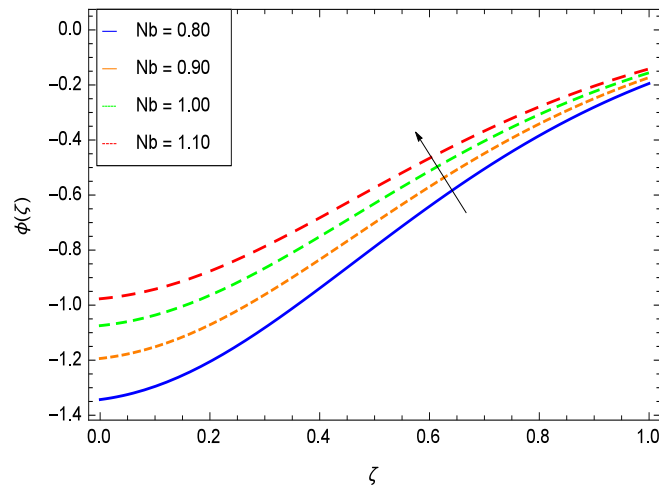


Figure 31. Effect on concentration profile for $h = -3.00$, $\gamma_1 = 0.50$, $\gamma_2 = 0.60$, $\gamma_3 = 0.20$, $\gamma_4 = 0.30$, $\gamma_5 = 1.00$, $Nr = 0.60$, $Rb = 0.70$, $Nt = 0.90$, $Le = 0.60$, $Sc = 0.70$, $Pe = 1.00$, $M = 1.00$, $Pr = 10.00$ and different values of Nb .

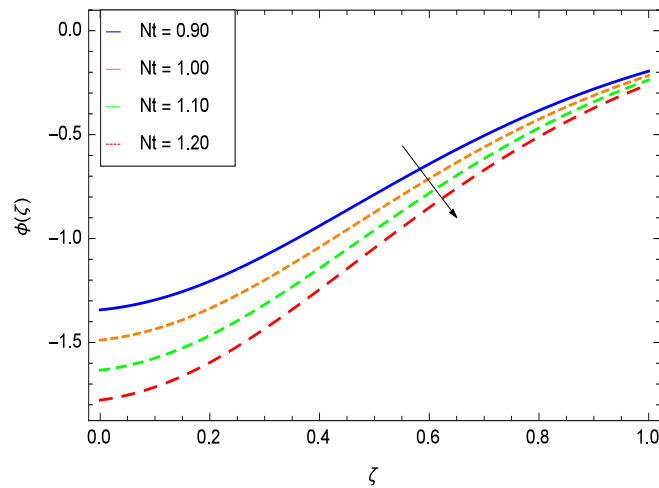


Figure 32. Effect on concentration profile for $h = -.00$, $\gamma_1 = 0.50$, $\gamma_2 = 0.60$, $\gamma_3 = 0.20$, $\gamma_4 = 0.30$, $\gamma_5 = 1.00$, $Nr = 0.60$, $Rb = 0.70$, $Nb = 0.90$, $Le = 0.60$, $Sc = 0.70$, $Pe = 1.00$, $M = 1.00$, $Pr = 10.00$ and different values of Nt .

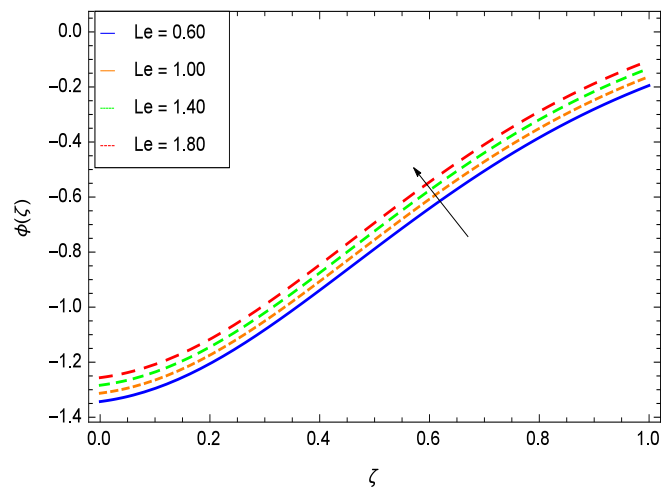


Figure 33. Effect on concentration profile for $h = -3.00$, $\gamma_1 = 0.50$, $\gamma_2 = 0.60$, $\gamma_3 = 0.20$, $\gamma_4 = 0.30$, $\gamma_5 = 1.00$, $Nr = 0.60$, $Rb = 0.70$, $Nb = 0.80$, $Nt = 0.90$, $Sc = 0.70$, $Pe = 1.00$, $M = 1.00$, $Pr = 10.00$ and different values of Le .

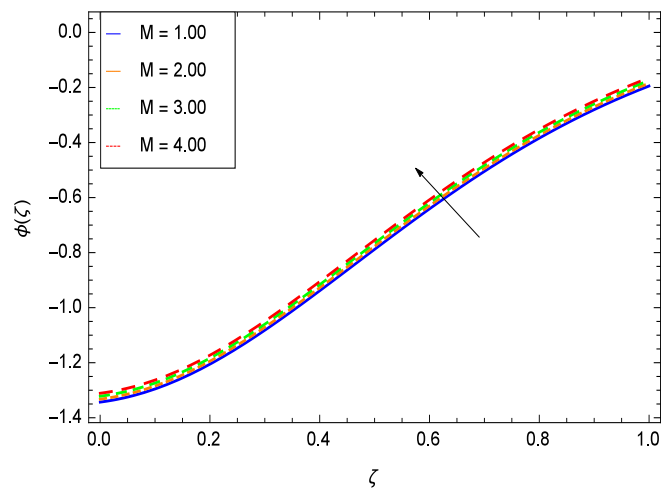


Figure 34. Effect on concentration profile for $h = -3.00$, $\gamma_1 = 0.50$, $\gamma_2 = 0.60$, $\gamma_3 = 0.20$, $\gamma_4 = 0.30$, $\gamma_5 = 1.00$, $Nr = 0.60$, $Rb = 0.70$, $Nb = 0.80$, $Nt = 0.90$, $Le = 0.60$, $Sc = 0.70$, $Pe = 1.00$, $Pr = 10.00$ and different values of M .

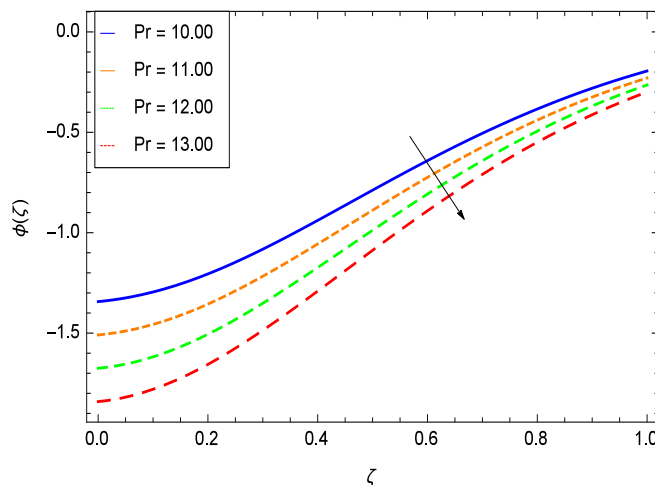


Figure 35. Effect on concentration profile for $h = -3.00$, $\gamma_1 = 0.50$, $\gamma_2 = 0.60$, $\gamma_3 = 0.20$, $\gamma_4 = 0.30$, $\gamma_5 = 1.00$, $Nr = 0.60$, $Rb = 0.70$, $Nb = 0.80$, $Nt = 0.90$, $Le = 0.60$, $Sc = 0.70$, $Pe = 1.00$, $M = 1.00$ and different values of Pr .

6.4. Gyrotactic Microorganism Concentration

There have been tremendous developments in the field of microorganism produced nanoparticles and their applications. The characteristics of the density motile microorganisms with respect to different parameters are discussed in the following. Figure 36 elucidates that the microorganism concentration profile $\Omega(\zeta)$ grows up with increasing magnitude of second grade nanofluid parameter γ_1 . The reason is that increasing the quantity γ_1 increases the microorganism propulsion by providing the best platform for the growth of microorganism and hence explains the reason why the microorganism concentration boundary layer of second grade nanofluid enhances. Figure 37 shows the influence of reduced heat parameter γ_2 on the microorganism concentration $\Omega(\zeta)$ profile. Intensity of temperature is not good for the survival of microorganism concentration. Therefore, in the present case, the microorganism concentration $\Omega(\zeta)$ increases with moderate temperature. Figure 38 projects that the the microorganism concentration $\Omega(\zeta)$ decreases with amplifying the porosity parameter γ_3 . In porous medium there is a resistance of holes to the flow of microorganisms so their progress is not significant in that case. Figure 39 illustrates that the non-dimensional microorganism concentration $\Omega(\zeta)$ profile depreciates with the rising values of inertial parameter γ_4 . This is due to the fact that the inertial parameter affects the motion of the microorganisms since the environment is not clear to them. Figure 40 reveals that microorganism concentration field $\Omega(\zeta)$ amplifies with the chemical reaction parameter γ_5 . Figure 41 shows that the microorganism concentration $\Omega(\zeta)$ decreases against the Brownian motion parameter Nb because the propulsion of microorganisms is weak. Figure 42 demonstrates that by increasing thermophoresis parameter Nt , the microorganism concentration profile $\Omega(\zeta)$ increases. This is due to the close relation of concentration with moderate temperature and it is expected that a higher thermophoresis parameter allows a deeper penetration of the microorganism concentration. This achieves enhancement in species in the nanofluid and elevates the motile microorganism concentration profile $\Omega(\zeta)$. This indicates that a stronger thermophoresis effect induces a resistance in the mass diffusion. In Figure 43, the microorganism concentration field $\Omega(\zeta)$ shows an upshot for the greater values of Lewis number Le . This happens because as the Lewis number Le increases, the viscous diffusion rate increases which in turn reduces the velocity at the surface and so elevates the density of the microorganisms. The effect of Schmidt number Sc on the microorganism concentration profile $\Omega(\zeta)$ is projected in Figure 44. When the magnitude of Schmidt number Sc increases, the microorganism concentration profile $\Omega(\zeta)$ decreases. This is attributed to the low propulsion of

microorganisms. Figure 45 shows the effect of bioconvection Peclet number Pe on the microorganism concentration profile $\Omega(\zeta)$. It indicates that the microorganism concentration profile $\Omega(\zeta)$ grows large for different values of bioconvection Peclet number Pe . This is due to the fact that microorganisms diffuse more and more with larger values of bioconvection Peclet number Pe . The bioconvection Peclet number Pe helps to increase the speed of the microorganisms in respect of the nanofluid and so the density of the microorganisms is reduced near the surface. The behavior is highly influenced with an increase in the Lewis number Le which again helps in the reduction of the mass diffusivity. Figure 46 shows that by increasing magnetic field parameter M , the nondimensional motile density function profile $\Omega(\zeta)$ decreases because the magnetic field opposes the flow due to Lorentz force.

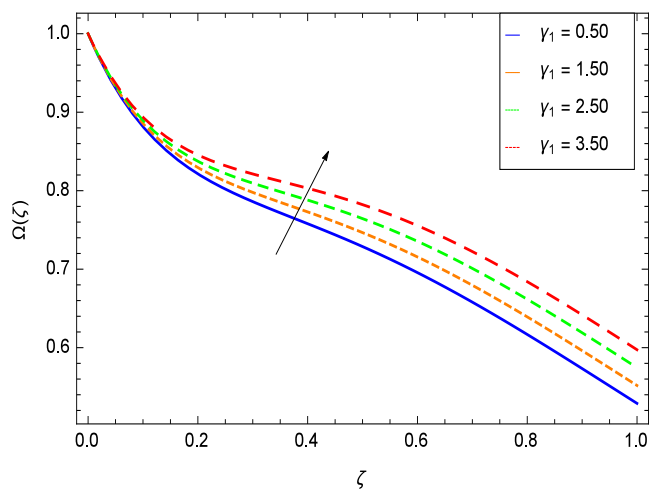


Figure 36. Effect on microorganisms density function for $h = -3.00, \gamma_2 = 0.60, \gamma_3 = 0.20, \gamma_4 = 0.30, \gamma_5 = 1.00, Gr = 0.50, Nr = 0.60, Rb = 0.70, Nb = 0.80, Nt = 0.90, Le = 0.60, Sc = 0.70, Pe = 1.00, M = 1.00, Pr = 10.00$ and different values of γ_1 .

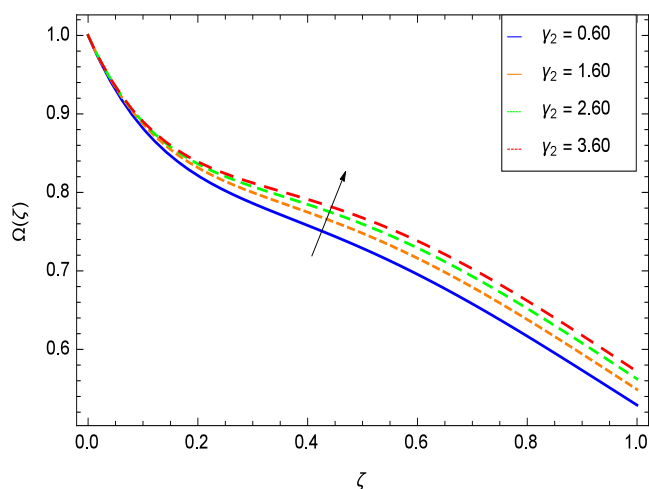


Figure 37. Effect on microorganisms density function for $h = -3.00, \gamma_1 = 0.50, \gamma_3 = 0.20, \gamma_4 = 0.30, \gamma_5 = 1.00, Gr = 0.50, Nr = 0.60, Rb = 0.70, Nb = 0.80, Nt = 0.90, Le = 0.60, Sc = 0.70, Pe = 1.00, M = 1.00, Pr = 10.00$ and different values of γ_2 .

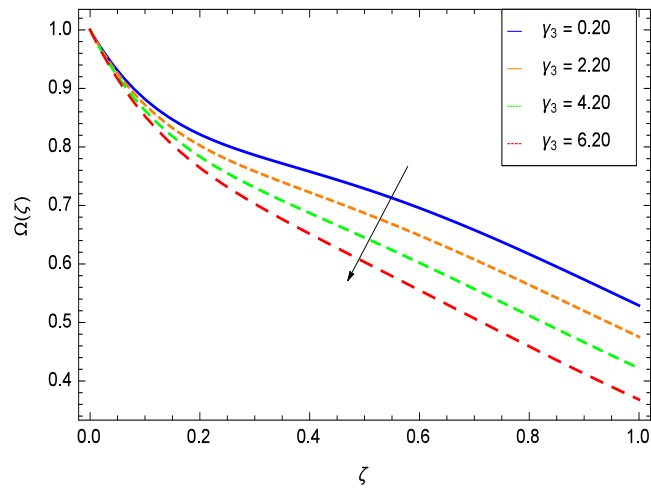


Figure 38. Effect on microorganisms density function for $h = -3.00$, $\gamma_1 = 0.50$, $\gamma_2 = 0.60$, $\gamma_4 = 0.30$, $\gamma_5 = 1.00$, $Gr = 0.50$, $Nr = 0.60$, $Rb = 0.70$, $Nb = 0.80$, $Nt = 0.90$, $Le = 0.60$, $Sc = 0.70$, $Pe = 1.00$, $M = 1.00$, $Pr = 10.00$ and different values of γ_3 .

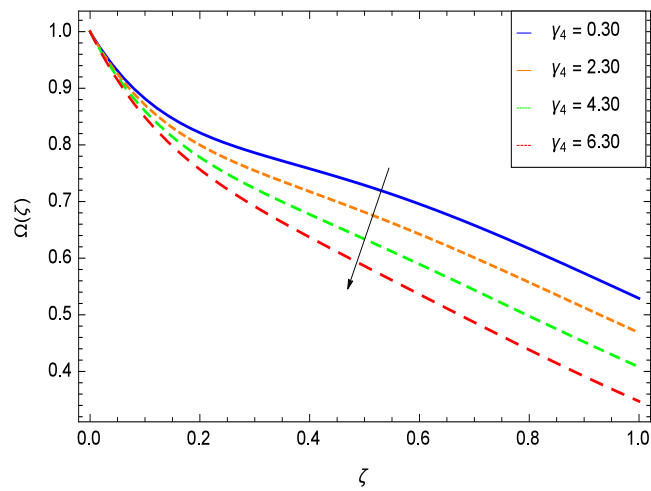


Figure 39. Effect on microorganisms density function for $h = -3.00$, $\gamma_1 = 0.50$, $\gamma_3 = 0.20$, $\gamma_2 = 0.60$, $\gamma_5 = 1.00$, $Gr = 0.50$, $Nr = 0.60$, $Rb = 0.70$, $Nb = 0.80$, $Nt = 0.90$, $Le = 0.60$, $Sc = 0.70$, $Pe = 1.00$, $M = 1.00$, $Pr = 10.00$ and different values of γ_4 .

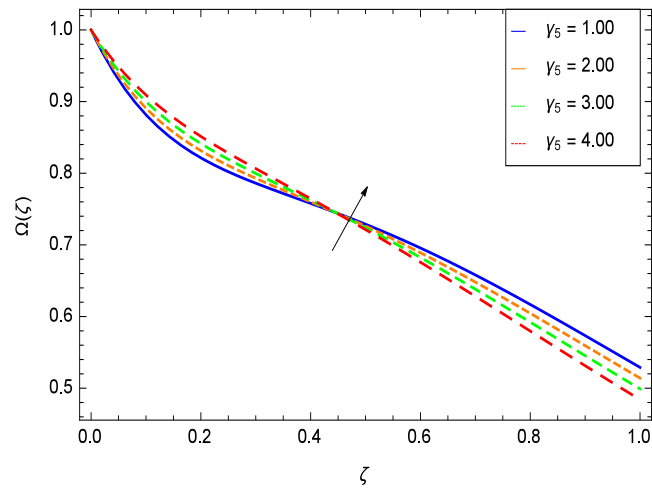


Figure 40. Effect on microorganisms density function for $h = -3.00$, $\gamma_1 = 0.50$, $\gamma_3 = 0.20$, $\gamma_2 = 0.60$, $\gamma_4 = 0.30$, $Gr = 0.50$, $Nr = 0.60$, $Rb = 0.70$, $Nb = 0.80$, $Nt = 0.90$, $Le = 0.60$, $Sc = 0.70$, $Pe = 1.00$, $M = 1.00$, $Pr = 10.00$ and different values of γ_5 .

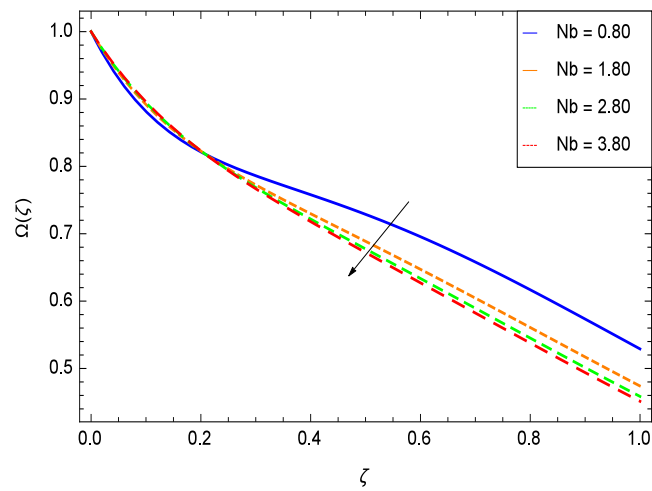


Figure 41. Effect on microorganisms density function for $h = -3.00$, $\gamma_1 = 0.50$, $\gamma_2 = 0.60$, $\gamma_3 = 0.20$, $\gamma_4 = 0.30$, $\gamma_5 = 1.00$, $Gr = 0.50$, $Nr = 0.60$, $Rb = 0.70$, $Nt = 0.90$, $Le = 0.60$, $Sc = 0.70$, $Pe = 1.00$, $M = 1.00$, $Pr = 10.00$ and different values of Nb .

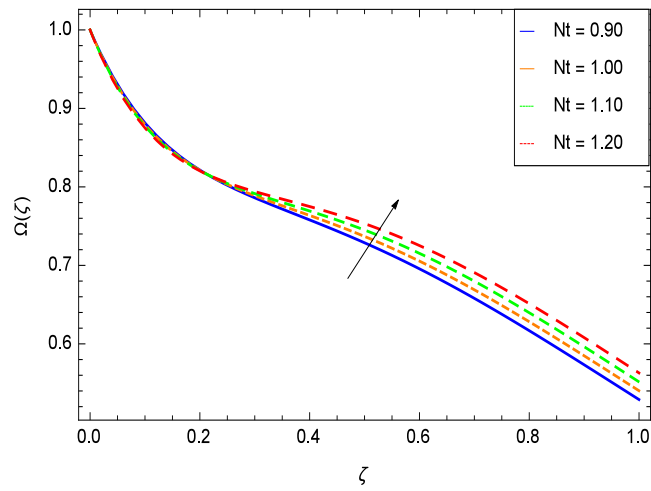


Figure 42. Effect on microorganisms density function for $h = -3.00$, $\gamma_1 = 0.50$, $\gamma_2 = 0.60$, $\gamma_3 = 0.20$, $\gamma_4 = 0.30$, $\gamma_5 = 1.00$, $Gr = 0.50$, $Nr = 0.60$, $Rb = 0.70$, $Nb = 0.80$, $Le = 0.60$, $Sc = 0.70$, $Pe = 1.00$, $M = 1.00$, $Pr = 10.00$ and different values of Nt .

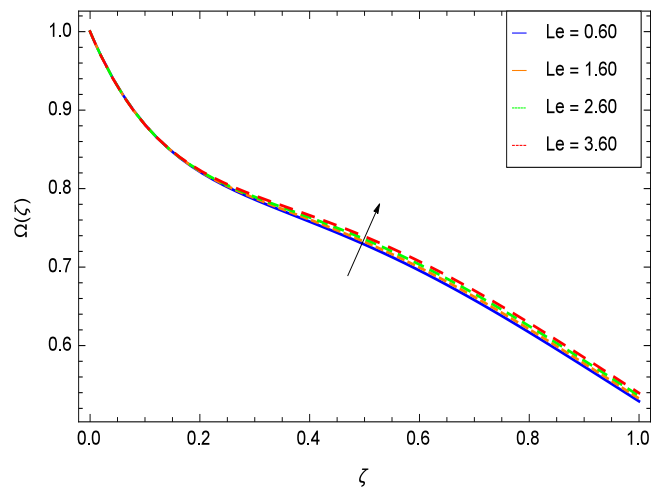


Figure 43. Effect on microorganisms density function for $h = -3.00$, $\gamma_1 = 0.50$, $\gamma_2 = 0.60$, $\gamma_3 = 0.20$, $\gamma_4 = 0.30$, $\gamma_5 = 1.00$, $Gr = 0.50$, $Nr = 0.60$, $Rb = 0.70$, $Nt = 0.90$, $Nb = 0.80$, $Sc = 0.70$, $Pe = 1.00$, $M = 1.00$, $Pr = 10.00$ and different values of Le .

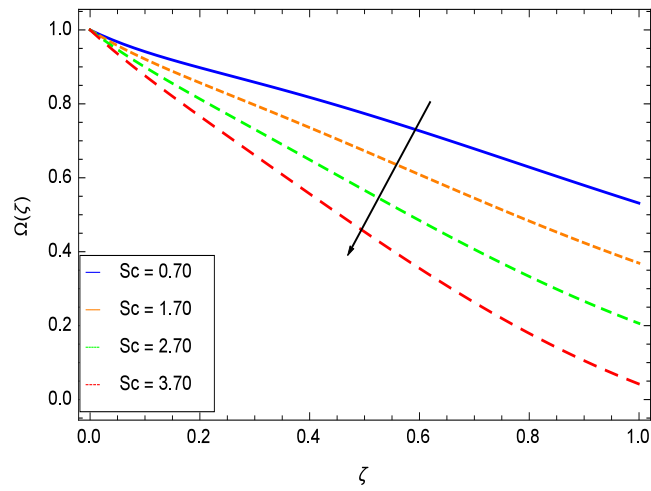


Figure 44. Effect on microorganisms density function for $h = -3.00$, $\gamma_1 = 0.50$, $\gamma_2 = 0.60$, $\gamma_3 = 0.20$, $\gamma_4 = 0.30$, $\gamma_5 = 1.00$, $Gr = 0.50$, $Nr = 0.60$, $Nb = 0.80$, $Nt = 0.90$, $Le = 0.60$, $Pe = 1.00$, $M = 1.00$, $Pr = 10.00$ and different values of Sc .

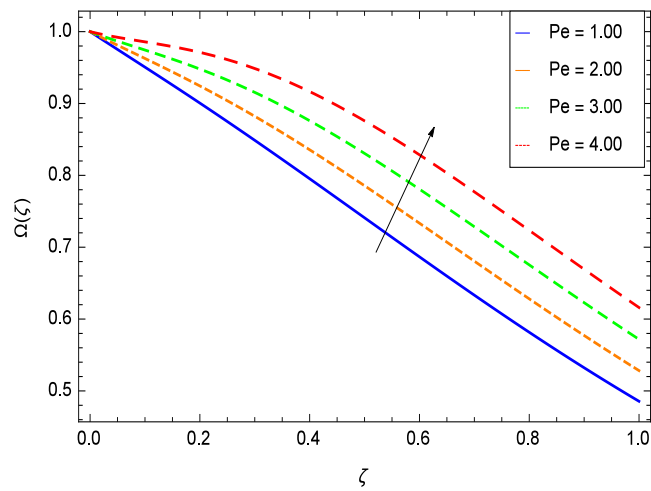


Figure 45. Effect on microorganisms density function for $h = -1.10$, $\gamma_1 = 0.50$, $\gamma_2 = 0.60$, $\gamma_3 = 0.20$, $\gamma_4 = 0.30$, $\gamma_5 = 1.00$, $Gr = 0.50$, $Nr = 0.60$, $Rb = 0.70$, $Nt = 0.90$, $Sc = 0.70$, $Nb = 0.80$, $M = 1.00$, $Pr = 10.00$ and different values of Pe .

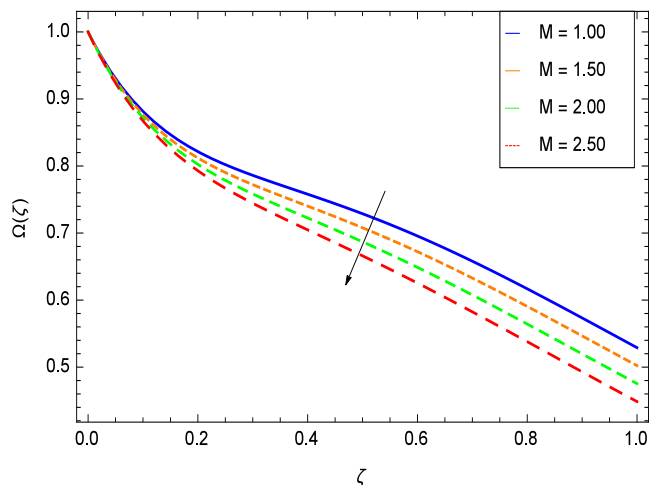


Figure 46. Effect on microorganisms density function for $h = -3.00$, $\gamma_1 = 0.50$, $\gamma_2 = 0.60$, $\gamma_3 = 0.20$, $\gamma_4 = 0.30$, $\gamma_5 = 1.00$, $Gr = 0.50$, $Nr = 0.60$, $Rb = 0.70$, $Nt = 0.90$, $Sc = 0.70$, $Nb = 0.80$, $Pe = 1.00$, $Pr = 10.00$ and different values of M .

7. Entropy Generation Analysis

It is necessary to study the irreversibility of the present system in terms of second-grade nanofluid, nanoparticles and microorganisms. Figure 47 shows that the irreversibility $N_G(\zeta)$ of the system increases for high values of Reynolds number Re . Similarly, the values of Br make enhancement in entropy generation rate $N_G(\zeta)$ which has the same increasing behavior in Figure 48. Different values of magnetic field parameter M in Figure 49 presents an increasing effect on the entropy generation rate $N_G(\zeta)$. In Figure 50, the nondimensional diffusive constant parameter γ_6 assumes various high values (ranging from 0.50 to 1.20) with deep effects observations. γ_6 is related to the diffusivity. It shows that entropy generation rate $N_G(\zeta)$ increases with increasing γ_6 where at the same time the temperature difference parameter θ_w reveals a unique activity, including the depreciation of entropy generation rate $N_G(\zeta)$ in Figure 51. The formation of curves of the entropy generation rate $N_G(\zeta)$ in Figure 52 is due to the various values of the concentration difference parameter ϕ_w , a reactive species making increment in $N_G(\zeta)$. In Figure 53, it is shown that microorganisms concentration difference parameter Ω_w favors the entropy generation rate.

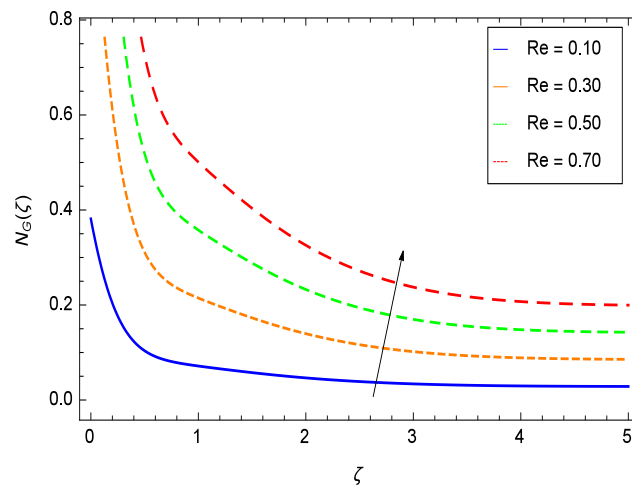


Figure 47. Effect on entropy generation rate for $h = -1.50$, $Br = 0.40$, $M = 0.50$, $\gamma_6 = 0.60$, $\theta_w = 0.70$, $\phi_w = 0.80$, $\Omega_w = 0.90$ and different values of Re .

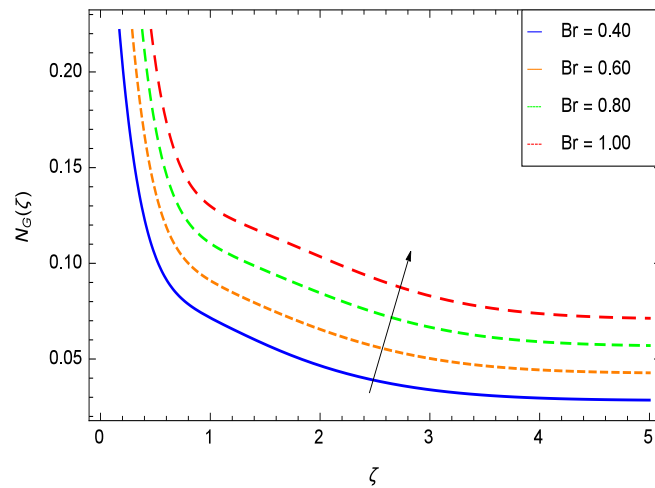


Figure 48. Effect on entropy generation rate for $h = -1.50$, $Re = 0.10$, $M = 0.50$, $\gamma_6 = 0.60$, $\theta_w = 0.70$, $\phi_w = 0.80$, $\Omega_w = 0.90$ and different values of Br .

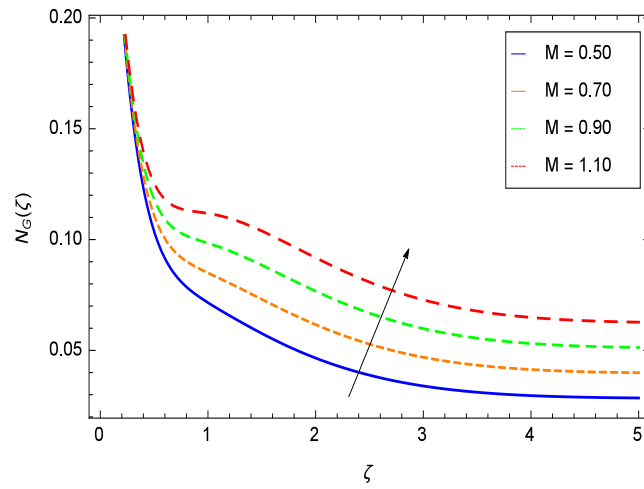


Figure 49. Effect on entropy generation rate for $h = -1.50$, $Re = 0.10$, $Br = 0.40$, $\gamma_6 = 0.60$, $\theta_w = 0.70$, $\phi_w = 0.80$, $\Omega_w = 0.90$ and different values of M .

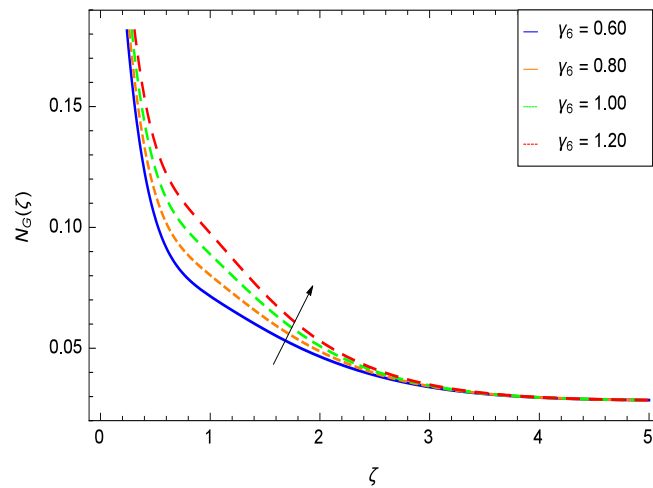


Figure 50. Effect on entropy generation rate for $h = -1.50$, $Re = 0.10$, $Br = 0.40$, $M = 0.50$, $\theta_w = 0.70$, $\phi_w = 0.80$, $\Omega_w = 0.90$ and different values of γ_6 .

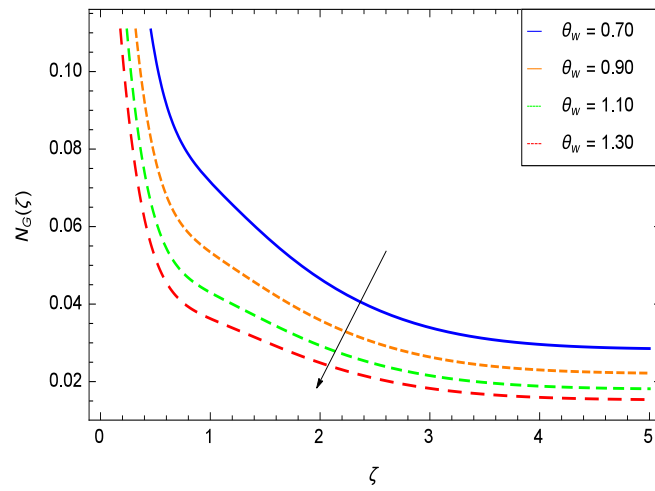


Figure 51. Effect on entropy generation rate for $h = -1.50$, $Re = 0.10$, $Br = 0.40$, $M = 0.50$, $\gamma_6 = 0.60$, $\phi_w = 0.80$, $\Omega_w = 0.90$ and different values of θ_w .

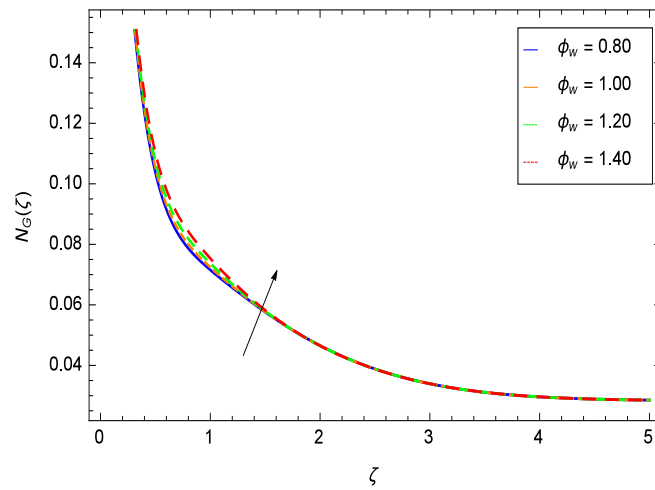


Figure 52. Effect on entropy generation rate for $h = -1.50$, $Re = 0.10$, $Br = 0.40$, $M = 0.50$, $\gamma_6 = 0.60$, $\theta_w = 0.70$, $\Omega_w = 0.90$ and different values of ϕ_w .

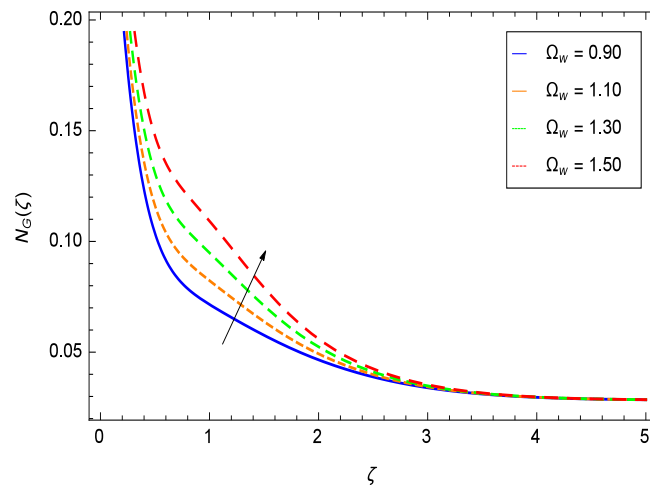


Figure 53. Effect on entropy generation rate for $h = -1.50$, $Re = 0.10$, $Br = 0.40$, $M = 0.50$, $\gamma_6 = 0.60$, $\theta_w = 0.70$, $\phi_w = 0.80$ and different values of Ω_w .

8. Residual Errors

Residual errors are shown in the graphs to show the authentication of the problem. By fixing all the others parameters, different values are assigned to convergence control parameter h to show the effects in Figures 54–57.

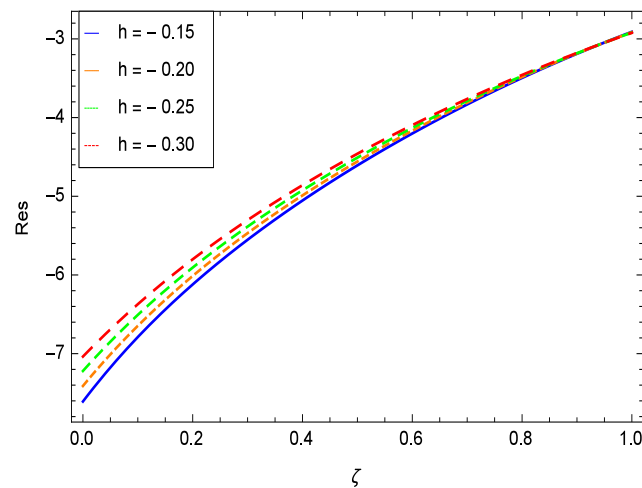


Figure 54. Residual errors graph of velocity profile for $\gamma = 0.30$, $\gamma_1 = 0.30$, $\gamma_2 = 0.30$, $\gamma_3 = 0.30$, $\gamma_4 = 0.30$, $Gr = 0.40$, $Nr = 0.40$, $Rb = 0.50$, $Nb = 0.50$, $Nt = 0.60$, $Le = 0.60$, $Sc = 0.40$, $Pe = 0.40$, $Pr = 0.70$, $M = 0.60$ and different values of h .

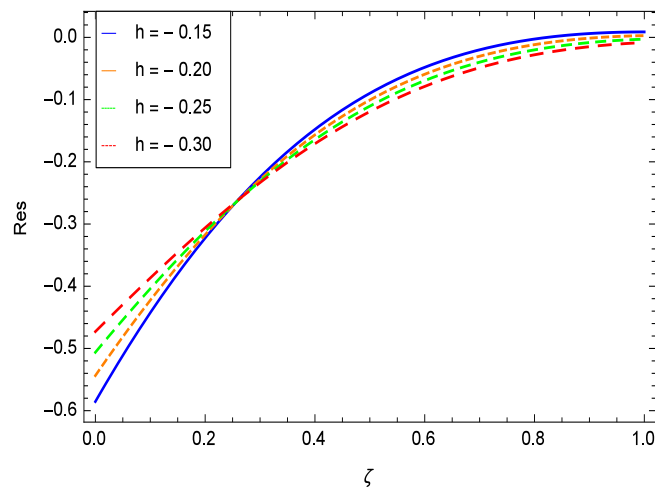


Figure 55. Residual errors graph of temperature profile for $\gamma = 0.30$, $\gamma_1 = 0.30$, $\gamma_2 = 0.30$, $\gamma_3 = 0.30$, $\gamma_4 = 0.30$, $Gr = 0.40$, $Nr = 0.40$, $Rb = 0.50$, $Nb = 0.50$, $Nt = 0.60$, $Le = 0.60$, $Sc = 0.40$, $Pe = 0.40$, $Pr = 0.70$, $M = 0.60$ and different values of h .

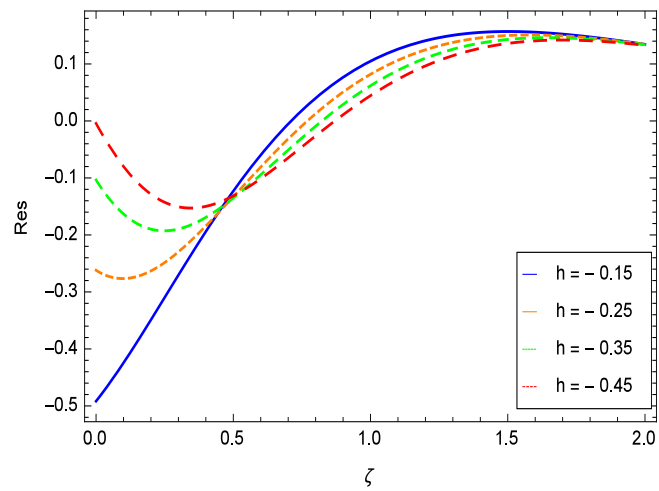


Figure 56. Residual errors graph of concentration profile for $\gamma = 0.30$, $\gamma_1 = 0.30$, $\gamma_2 = 0.30$, $\gamma_3 = 0.30$, $\gamma_4 = 0.30$, $Gr = 0.40$, $Nr = 0.40$, $Rb = 0.50$, $Nb = 0.50$, $Nt = 0.60$, $Le = 0.60$, $Sc = 0.40$, $Pe = 0.40$, $Pr = 0.70$, $M = 0.60$ and different values of h .

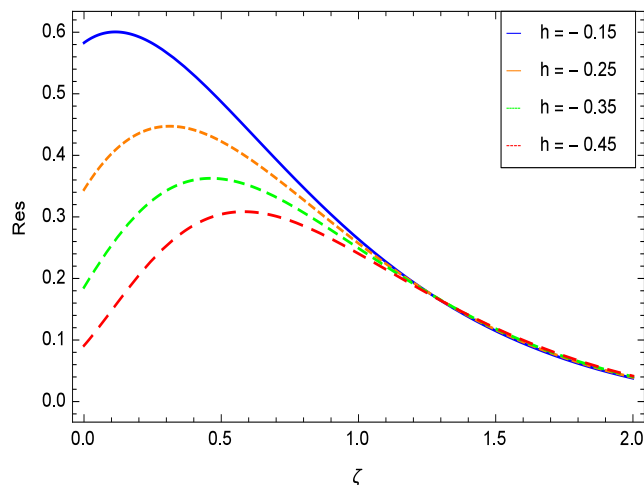


Figure 57. Residual errors graph of microorganism concentration profile for $\gamma = 0.30$, $\gamma_1 = 0.30$, $\gamma_2 = 0.30$, $\gamma_3 = 0.30$, $\gamma_4 = 0.30$, $Gr = 0.40$, $Nr = 0.40$, $Rb = 0.50$, $Nb = 0.50$, $Nt = 0.60$, $Le = 0.60$, $Sc = 0.40$, $Pe = 0.40$, $Pr = 0.70$, $M = 0.60$ and different values of h .

9. Conclusions

This article discusses the analytical solution of entropy generation and mixed convection in gravity-driven non-Newtonian second grade nanofluid flow containing both nanoparticles and gyrotactic microorganisms through a porous medium with a chemical reaction along a convectively heated vertical solid surface. The thin film considered in this work contains the mixture of nanoparticles and motile gyrotactic microorganisms [14]. The solution of the problem has been obtained by using analytical technique called Homotopy Analysis Method (HAM) for the velocity, temperature, concentration and microorganism concentration fields, which has been displayed in the diagrams. From Figures 6–53, each figure displays the profound effect of the emerging parameters on the flow, heat transfer, nanoparticles concentration, microorganism concentration and entropy generation. Residual errors sketches are drawn in Figures 54–57 to show the authentication of the HAM solution. The main findings of the study are summarized as following.

- (i) The velocity $f(\zeta)$ depreciates for the porosity parameter γ_3 , inertial parameter γ_4 , bioconvection Rayleigh number Rb and magnetic field parameter M while it elevates for the second grade nanofluid parameter γ_1 , reduced heat transfer parameter γ_2 , chemical reaction parameter γ_5 , buoyancy parameter Gr , buoyancy ratio parameter Nr , Lewis number Le , Schmidt number Sc and Prandtl number Pr .
- (ii) The temperature $\theta(\zeta)$ diminishes for the reduced heat transfer parameter γ_2 , porosity parameter γ_3 , inertial parameter γ_4 , magnetic field parameter M and Prandtl number Pr while it elevates for the second grade nanofluid parameter γ_1 , chemical reaction parameter γ_5 and thermophoresis parameter Nt .
- (iii) The nanoparticles concentration $\phi(\zeta)$ diminishes for second grade nanofluid parameter γ_1 , reduced heat transfer parameter γ_2 , thermophoresis parameter Nt and Prandtl number Pr while it elevates for the porosity parameter γ_3 , inertial parameter γ_4 , chemical reaction parameter γ_5 , Brownian motion parameter Nb , Lewis number Le and magnetic field parameter M .
- (iv) The microorganism concentration $\Omega(\zeta)$ diminishes for the porosity parameter γ_3 , inertial parameter γ_4 , Brownian motion parameter Nb , Schmidt number Sc and magnetic field parameter M while it

- elevates for the second grade nanofluid parameter γ_1 , reduced heat parameter γ_2 , chemical reaction parameter γ_5 , Lewis number Le , thermophoresis parameter Nt and bioconvection Peclet number Pe .
- (v) Entropy generation rate $N_G(\zeta)$ diminishes with temperature difference parameter θ_w while it elevates for Reynolds number Re , Brinkman number Br , magnetic field parameter M , diffusive constant parameter γ_6 , nanoparticles concentration difference parameter ϕ_w and microorganism concentration difference parameter Ω_w .
- (vi) Residual errors graphs are self explanatory for the efficiency of HAM solution.

Author Contributions: Conceptualization, N.S.K.; methodology, N.S.K.; software, Z.S.; validation, S.I.; formal analysis, I.K.; investigation, I.T.; resources, N.S.K.; data curation, I.T.; writing—original draft preparation, N.S.K.; writing—review and editing, T.A.A.; visualization, T.A.A.; supervision, N.S.K.

Funding: This research received no external funding.

Acknowledgments: The authors are thankful to the Higher Education Commission (HEC) Pakistan for providing the technical and financial support. The authors also express their deep and hearty thanks to the honorable reviewers for useful comments and information on the literature.

Conflicts of Interest: The authors declare no conflict of interest.

Abbreviations

The following abbreviations are used in this manuscript:

x	x -axis coordinate (m)
y	y -axis coordinate (m)
u	Velocity component along x -axis (m s^{-1})
v	Velocity component along y -axis (m s^{-1})
\bar{v}	Average swimming velocity (m s^{-1})
U	Free stream velocity (m s^{-1})
W_c	Maximum cell swimming speed (m s^{-1})
a	Constant
b	Chemotaxis constant
B_0	Magnetic flux density (Tesla)
Gr	Thermal Grashof number
M	Magnetic field parameter
Nr	Buoyancy ratio parameter
Rb	Bioconvection Rayleigh number
Nt	Thermophoresis parameter
Nb	Brownian motion parameter
Le	Lewis number
Sc	Schmidt number
Pe	Bioconvection Peclet number
Pr	Prandtl number
g	Gravitational acceleration (m s^{-2})
P	Pressure ($\text{kg m}^{-1} \text{s}^{-2}$)
c_p	Specific heat at constant pressure ($\text{J kg}^{-1} \text{K}^{-1}$)
k	Thermal conductivity (W/m K)
T	Temperature (K)
T_f	Convective surface temperature (K)
T_∞	Ambient fluid temperature (K)
h_f	Heat transfer coefficient
C	Nanoparticles concentration
C_∞	Ambient fluid concentration

N	Number density of motile microorganisms
N_w	Wall concentration of microorganisms
N_∞	Ambient concentration of microorganisms
N_G	Entropy generation number
D	Diffusivity
D_B	Brownian diffusion coefficient
D_T	Thermophoretic diffusion coefficient
D_n	Diffusivity of microorganisms
$f(\zeta)$	Dimensionless velocity
L	Characteristic length (m)
R	Ideal gas constant
Re	Reynolds number
Br	Brinkman number
α_1	Normal stress moduli
σ	Electrical conductivity ($(\Omega \cdot m)^{-1}$)
μ	Coefficient of viscosity ($kg\ m^{-1}\ s^{-1}$)
ρ	Density ($kg\ m^{-3}$)
ν	Kinematic viscosity ($m^2\ s^{-1}$)
ψ	Physical stream function ($m^2\ s^{-1}$)
β	Coefficient of volumetric volume expansion
Δ	Difference operator
λ	Thermal diffusivity of nanofluid ($m^2\ s^{-1}$)
τ	Ratio of the heat capacitances of nanoparticle and base fluid
ζ	A scaled boundary layer coordinate
$\theta(\zeta)$	Dimensionless temperature
θ_w	Dimensionless temperature difference
$\phi(\zeta)$	Dimensionless concentration
ϕ_w	Dimensionless concentration difference
$\Omega(\zeta)$	Dimensionless microorganisms concentration
Ω_w	Dimensionless microorganisms concentration difference
γ_{av}	Average volume of microorganisms (m^{-3})
γ_1	Dimensionless second grade nanofluid parameter
γ_2	Reduced heat transfer parameter
γ_3	Porosity parameter
γ_4	Inertial parameter
γ_5	Chemical reaction parameter
γ_6	Diffusive constant parameter due to nanoparticles concentration
γ_7	Non-dimensional positive number
γ_8	Diffusive constant parameter due to microorganisms concentration
av	Average
B	Brownian
c	Cell
p	Solid particles
r	Reaction
n	Properties related to microorganisms
f	Base fluid
o	Origin
x	Local value
w	Properties at the wall
∞	Fluid properties at ambient condition
Superscripts	
s	Swimming
/	Differentiation w. r. t. ζ

References

1. Khan, N.S.; Zuhra, Z.; Shah, Z.; Bonyah, E.; Khan, W.; Islam, S. Hall current and thermophoresis effects on magnetohydrodynamic mixed convective heat and mass transfer thin film flow. *J. Phys. Commun.* **2018**. [[CrossRef](#)]
2. Ishaq, M.; Ali, M.; Shah, Z.; Islam, S.; Muhammad, S. Entropy generation on nanofluid thin film flow of Eyring-Powell fluid with thermal radiation and MHD effect on an unsteady porous stretching sheet. *Entropy* **2018**. [[CrossRef](#)]
3. Hayat, T.; Khan, M. I.; Qayyum, S.; Khan, M. I.; Alsaedi, A. Entropy generation for flow of Sisko fluid to rotating disk. *J. Mol. Liquids* **2018**, *264*, 375–385 [[CrossRef](#)]
4. Khan, N.S.; Gul, T.; Khan, M.A.; Bonyah, E.; Islam, S. Mixed convection in gravity-driven thin film non-Newtonian nanofluids flow with gyrotactic microorganisms. *Results Phys.* **2017**, *7*, 4033–4049. [[CrossRef](#)]
5. Zuhra, S.; Khan, N.S.; Islam, S. Magnetohydrodynamic second grade nanofluid flow containing nanoparticles and gyrotactic microorganisms. *Comput. Appl. Math.* **2018**, *37*, 6332–6358. [[CrossRef](#)]
6. Khan, N.S. Bioconvection in second grade nanofluid flow containing nanoparticles and gyrotactic microorganisms. *Braz. J. Phys.* **2018**, *43*, 227–241. [[CrossRef](#)]
7. Palwasha, Z.; Islam, S.; Khan, N.S.; Ayaz, H. Non-Newtonian nanoliquids thin film flow through a porous medium with magnetotactic microorganisms. *Appl. Nanosci.* **2018**, *8*, 1523–1544. [[CrossRef](#)]
8. Raees, A.; Xu, H.; Liao, S.J. Unsteady mixed nano-bioconvection flow in a horizontal channel with its upper plate expanding or contracting. *Int. J. Heat Mass Transf.* **2015**, *86*, 174–182. [[CrossRef](#)]
9. Zuhra, S.; Khan, N.S.; Shah, Z.; Islam, S.; Bonyah, E. Simulation of bioconvection in the suspension of second grade nanofluid containing nanoparticles and gyrotactic microorganisms. *AIP Adv.* **2018**, *8*, 105210. [[CrossRef](#)]
10. Pedley, T.J. Instability of uniform microorganism suspensions revisited. *J. Fluid Mech.* **2010**, *647*, 335–359. [[CrossRef](#)]
11. Xu, H.; Pop, I. Mixed convection flow of a nanofluid over a stretching surface with uniform free stream in the presence of both nanoparticles and gyrotactic microorganisms. *Int. J. Heat Mass Transf.* **2014**, *75*, 610–623. [[CrossRef](#)]
12. Aziz, A.; Khan, W.A.; Pop, I. Free convection boundary layer flow past a horizontal flat plate embedded in porous medium filled by nanofluid containing gyrotactic microorganisms. *Int. J. Therm. Sci.* **2012**, *56*, 48–57. [[CrossRef](#)]
13. Bhatti, M.M.; Mishra, S.R.; Abbas, T.; Rashidi, M.M. A mathematical model of MHD nanofluid flow having gyrotactic microorganisms with thermal radiation and chemical reaction effects. *Neural Comput. Appl.* **2016**. [[CrossRef](#)]
14. Raees, A.; Xu, H.; Sun, Q.; Pop, I. Mixed convection in gravity-driven nanoliquid film containing both nanoparticles and gyrotactic microorganisms. *Appl. Math. Mech.* **2015**, *36*, 163–178. [[CrossRef](#)]
15. Ramzan, M.; Chung, J.D. Naeem Ullah, Radiative magnetohydrodynamic nanofluid flow due to gyrotactic microorganisms with chemical reaction and non-linear thermal radiation. *Int. J. Mech. Sci.* **2017**. [[CrossRef](#)]
16. Anjalidevi, S.P.; Kandasamy, R. Effects of chemical reaction, heat and mass transfer on laminar flow along a semi infinite horizontal plate. *Heat Mass Transf.* **1999**, *35*, 465–467. [[CrossRef](#)]
17. Khan, N.S.; Gul, T.; Islam, S.; Khan, W. Thermophoresis and thermal radiation with heat and mass transfer in a magnetohydrodynamic thin film second-grade fluid of variable properties past a stretching sheet. *Eur. Phys. J. Plus* **2017**, *132*. [[CrossRef](#)]
18. Palwasha, Z.; Khan, N.S.; Shah, Z.; Islam, S.; Bonyah, E. Study of two-dimensional boundary layer thin film fluid flow with variable thermophysical properties in three dimensions space. *AIP Adv.* **2018**, *8*, 105318. [[CrossRef](#)]
19. Khan, N.S.; Zuhra, S.; Shah, Z.; Bonyah, E.; Khan, W.; Islam, S. Slip flow of Eyring-Powell nanoliquid film containing graphene nanoparticles. *AIP Adv.* **2018**, *8*, 115302. [[CrossRef](#)]
20. Zuhra, S.; Khan, N.S.; Khan, M.A.; Islam, S.; Khan, W.; Bonyah, E. Flow and heat transfer in water based liquid film fluids dispensed with graphene nanoparticles. *Results Phys.* **2018**, *8*, 1143–1157. [[CrossRef](#)]

21. Khan, N.S.; Gul, T.; Islam, S.; Khan, I.; Alqahtani, A.M.; Alshomrani, A.S. Magneto hydrodynamic nanoliquid thin film sprayed on a stretching cylinder with heat transfer. *J. Appl. Sci.* **2017**, *7*, 271. [[CrossRef](#)]
22. Khan, N.S.; Gul, T.; Islam, S.; Khan, A.; Shah, Z. Brownian motion and thermophoresis effects on MHD mixed convective thin film second-grade nanofluid flow with Hall effect and heat transfer past a stretching sheet. *J. Nanofluids* **2017**, *6*, 812–829. [[CrossRef](#)]
23. Khan, N.S.; Gul, T.; Islam, S.; Khan, W.; Khan, I.; Ali, L. Thin film flow of a second-grade fluid in a porous medium past a stretching sheet with heat transfer. *Alex. Eng. J.* **2017**. [[CrossRef](#)]
24. Wu, M.; Kuznetsov, A.V.; Jasper, W.J. Modeling of particle trajectories in an electro-statically charged channel. *Phys. Fluids* **2011**, *22*, 043301. [[CrossRef](#)]
25. Kuznetsov, A.V. *Emerging Topics in Heat and Mass Transfer in Porous Media, From Bioengineering and Microelectronics to Nanotechnology*; Springer: Dordrecht, The Netherlands, 2012.
26. Tham, L.; Nazar, R.; Pop, I. Steady mixed convection boundary layer flow on a horizontal circular cylinder with a constant surface temperature embedded in a porous medium saturated by a nanofluid containing both nanoparticles and gyrotactic microorganisms. *J. Heat Transf.* **2013**, *135*, 102601-1. [[CrossRef](#)]
27. Liao, S.J. *Homotopy Analysis Method in Nonlinear Differential Equations*; Higher Education Press: Beijing, China; Springer: Berlin/Heidelberg, Germany, 2012.



© 2019 by the authors. Licensee MDPI, Basel, Switzerland. This article is an open access article distributed under the terms and conditions of the Creative Commons Attribution (CC BY) license (<http://creativecommons.org/licenses/by/4.0/>).